HHS Public Access

Author manuscript

*Nature*. Author manuscript; available in PMC 2019 August 06.

Published in final edited form as:

*Nature*. 2019 February ; 566(7742): 73–78. doi:10.1038/s41586-018-0784-9.

# LINE-1 derepression in senescent cells triggers interferon and inflammaging

**Marco De Cecco**[1], **Takahiro Ito**[1], **Anna P. Petrashen**[1], **Amy E. Elias**[1], **Nicholas J. Skvir**[1], **Steven W. Criscione**[1], **Alberto Caligiana**[1,†], **Greta Brocculi**[1,†], **Emily M. Adney**[2,3], **Jef D. Boeke**[2], **Oanh Le**[4], **Christian Beauséjour**[4], **Jayakrishna Ambati**[5], **Kameshwari Ambati**[5], **Matthew Simon**[6], **Andrei Seluanov**[6], **Vera Gorbunova**[6], **P. Eline Slagboom**[7], **Stephen L. Helfand**[1], **Nicola Neretti**[1,8], and **John M. Sedivy**[1]

[1]Department of Molecular Biology, Cell Biology and Biochemistry, Brown University, Providence, Rhode Island 02912, USA. [2]Institute for Systems Genetics and Department of Biochemistry and Molecular Pharmacology, NYU Langone Health, New York, New York 10016, USA. [3]McKusick-Nathans Institute of Genetic Medicine, Johns Hopkins University School of Medicine, Baltimore, MD 21205, USA. [4]Centre de Recherche CHU Ste-Justine, and Department of Pharmacology and Physiology, Université de Montréal, 3175 Côte Ste-Catherine, Montréal, Québec H3T1C5, Canada. [5]Center for Advanced Vision Science and Department of Ophthalmology, University of Virginia School of Medicine, Charlottesville, Virginia 22908, USA. [6]Department of Biology, University of Rochester, Rochester, New York 14627, USA. [7]Department of Molecular Epidemiology, Leiden University Medical Centre, 2300 RC Leiden, The Netherlands. [8]Center for Computational Molecular Biology, Brown University, Providence, Rhode Island 02912, USA.

## Abstract

Retrotransposable elements (RTEs) are deleterious at multiple levels, and failure of host surveillance systems can thus have negative consequences. However, the contribution of RTE activity to aging and age-associated diseases is not known. Here we show that during cellular



**Author Information.** Correspondence and requests for materials should be addressed to john_sedivy@brown.edu.
† Present address: Department of Pharmacy and Biotechnology, University of Bologna, Bologna, Italy.

**Author Contributions.** J.M.S. conceived the study. J.M.S. and M.D. designed the experiments. M.D. and T.I. maintained cell cultures and performed lentiviral interventions. M.D. performed RT-qPCR in cell culture and mouse tissues with help from M.S. and G.B. T.I. and A.C. performed immunoblots. M.D. performed all IF analyses. N.J.S., S.W.C. and A.E.E. did the bioinformatics and statistics. A.P.P. performed IHC and tissue histology. E.M.A. generated and validated antibodies against murine Orf1. O.L. irradiated mice and harvested tissues. J.A. and K.A. provided NRTI analogs. P.E.S. provided human samples. J.D.B., C.B., J.A., K.A., A.S., V.G., P.E.S., S.L.H., N.N. and J.M.S. contributed to personnel supervision, data interpretation and critical analysis. J.M.S. and M.D. wrote the manuscript with feedback from all authors.

**Competing Financial Interests.** J.A. is a cofounder of iVeena Holdings, iVeena Delivery Systems, and Inflammasome Therapeutics, and has been a consultant for Allergan, Biogen, Boehringer-Ingelheim, Janssen, Olix Pharmaceuticals, and Saksin LifeSciences in a capacity unrelated to this work. J.A. and K.A. are named as inventors on patent applications on macular degeneration filed by the University of Kentucky or the University of Virginia. J.D.B is a founder and Director of Neochromosome, Inc., the Center of Excellence for Engineering Biology, and CDI Labs, Inc. He serves on the Scientific Advisory Boards of Modern Meadow, Inc., Recombinetics, Inc., and Sample6, Inc.

**Data availability.** All source data and exact *P* values (if applicable) for every figure are included in the supporting information that accompanies the paper. RNA-seq data are on the Gene Expression Omnibus (GEO) with accession number GSE109700. Any other data or information relevant to this study are available from the corresponding author upon reasonable request.

senescence LINE-1 elements (L1s) become transcriptionally derepressed and activate a type-I interferon (IFN-I) response. The IFN-I response is a novel phenotype of late senescence and contributes to the maintenance of the senescence associated secretory phenotype (SASP). The IFN-I response is triggered by cytoplasmic L1 cDNA, and is antagonized by nucleoside reverse transcriptase inhibitors (NRTIs) that inhibit the L1 reverse transcriptase (RT). Treatment of aged mice with the NRTI lamivudine downregulated IFN-I activation and age-associated inflammation in several tissues. We propose that RTE activation is an important component of sterile inflammation that is a hallmark of aging, and that L1 RT is a relevant target for the treatment of age-associated disorders.

RTE activity can promote aberrant transcription, alternative splicing, insertional mutagenesis, DNA damage and genome instability[1]. RTE-derived sequences comprise up to two thirds of the human genome[2], although the great majority were active millions of years ago and are no longer intact. The only human RTE capable of autonomous retrotransposition is the long-interspersed element-1 (LINE-1, or L1). However, germline activity of L1 is a major source of human structural polymorphisms[3]. Increasing evidence points to RTE activation in some cancers, in the adult brain, and during aging[4–7]. Cellular defenses include heterochromatinization of the elements, small RNA pathways that target the transcripts, and anti-viral innate immunity mechanisms[8]. Somatic activation of RTEs with age is conserved in yeast and *Drosophila* and reducing RTE activity has beneficial effects[8].

## Activation of L1 and interferon in cellular senescence

We show here that L1 transcription is activated exponentially during replicative senescence (RS) of human fibroblasts, increasing 4–5-fold by 16 weeks after cessation of proliferation, which we refer to as late senescence (Fig. 1a, Extended Data Fig. 1a-e). Multiple RT-qPCR primers were designed to detect evolutionarily recent L1 elements (L1HS-L1PA5; Fig. 1b, Extended Data Fig. 1h). Levels of L1 polyA+ RNA increased 4–5-fold in late senescent cells (RS) in the sense but not antisense direction throughout the entire element (Fig. 1c). We Sanger sequenced long-range RT-PCR amplicons (Fig. 1b) to identify 224 elements dispersed throughout the genome; one third (75, 33.5%) were L1HS, of which 19 (25.3%, 8.5% of total) were intact (i.e. are annotated to be free of ORF-inactivating mutations; Extended Data Fig. 1f, g). We also performed 5’RACE with the same primers and found that the majority of L1 transcripts upregulated in senescent cells initiated within or near the 5’UTR (Extended Data Fig. 2).

L1 elements can stimulate an IFN-I response[9]. We found that interferons IFN-α and IFN-β1 were induced to high levels in late senescent cells. (Fig. 1d, Extended Data Fig. 1i). Cellular senescence proceeds through an early DNA damage response phase followed by the SASP response[10]. We document here a third and even later phase, characterized by the upregulation of L1 and an IFN-I response (Fig. 1e), which has not been previously noted, probably because most studies have focused on earlier times. Whole transcriptome RNA-seq analysis confirmed that the SASP and IFN-I responses are temporally distinct (Extended Data Fig. 3). The late phase of L1 activation and IFN-I induction was also observed in

oncogene-induced senescence (OIS) and stress-induced premature senescence (SIPS) (Fig. 1e, Extended Data Fig. 1j, k).

## Mechanisms of L1 activation

To explore how surveillance fails during senescence we examined three factors: TREX1, RB1 and FOXA1. TREX1 is a 3' exonuclease that degrades foreign invading DNAs and its loss has been associated with the accumulation of cytoplasmic L1 cDNA[11]. We found that the expression of TREX1 was significantly decreased in senescent cells (Extended Data Fig. 4a). RB1 has been shown to bind to repetitive elements, including L1s, and promote their heterochromatinization[12]. We found that the expression of RB1 declined strongly in senescent cells (RS; Fig. 2a) while that of other RB family members (RBL1, RBL2) did not change (Extended Data Fig. 4b). RB1 enrichment in the 5'UTR of L1 elements was evident in proliferating cells, decreased in early senescence and became undetectable at later times (Fig. 2a). This coincided with a decrease of H3K9me3 and H3K27me3 marks in these regions (Extended Data Fig. 4c).

To identify novel factors that interact with the L1 5'UTR we examined the ENCODE ChIP-seq database and found that the pioneering transcription factor FOXA1 binds to this region in several cell lines (Extended Data Fig. 4d). FOXA1 is upregulated in senescent cells[13] and bound to the central region of the L1 5'UTR (Fig. 2b). Using transcriptional reporters we found that deletion of the FOXA1 binding site decreased both sense and antisense transcription from the L1 5' UTR[14] (Extended Data Fig. 4e). Hence, the observed misregulation of these three factors in senescent cells could promote the activation of L1 by three additive mechanisms: loss of RB1 by relieving heterochromatin repression, gain of FOXA1 by activating the L1 promoter, and loss of TREX1 by compromising the removal of L1 cDNA.

We thus tested the effects of manipulating RB1, FOXA1 or TREX1 expression in fully senescent cells using lentiviral vectors (Extended Data Fig. 5a, b). Ectopic expression of RB1 suppressed the elevated expression of L1, IFN-α and IFN-β1 in senescent cells, while its knockdown further enhanced their expression (Fig. 2d). RB1 overexpression also restored its occupancy of the L1 5'UTR (Fig. 2c). Conversely, knockdown of FOXA1 reduced its binding to the L1 5'UTR (Extended Data Fig. 4f) and decreased the expression of L1, IFN-α and IFN-β1, while overexpression of FOXA1 increased L1, IFN-α and IFN-β1 levels (Fig. 2e). Congruent results were also obtained by manipulating TREX1 (Fig. 2g). Hence, each of these factors had a tangible effect on regulating L1 and the IFN-I response in senescent cells.

Single or double interventions targeted at these factors elicited only modest changes in L1 and IFN-I expression in growing early passage cells. While some of these effects were statistically significant, they were dwarfed by a triple intervention of RB1 and TREX1 104knockdowns combined with FOXA1 overexpression (3X), which resulted in a massive induction of L1 and IFN-I expression (Fig. 2f, Extended Data Fig. 4g-i and 5c). Hence, in normal healthy cells all three effectors have to be compromised to effectively unleash L1.

## Consequences of L1 activation

To assess IFN-I activation by L1 in more detail we examined the expression of 84 genes in this pathway using PCR arrays. We observed a widespread response, with the majority of the genes being upregulated (Fig. 2h, Extended Data Fig. 4j, k): 68% (57/84) were significantly upregulated in senescent cells, and 52% (44/84) were upregulated in 3X cells. These data verify and further extend the RNA-seq transcriptomic analysis (Extended Data Fig. 3).

Some NRTIs developed against HIV have been found to also inhibit L1 RT activity[15]. We also developed shRNAs against L1, two of which reduced transcript levels by 40–50% and 70–90% in deeply senescent and 3X cells, respectively (Extended Data Fig. 5g). ORF1 protein levels were correspondingly reduced in deeply senescent cells (Extended Data Fig. 5h). Finally, the shRNAs also reduced the retrotransposition of recombinant L1 reporter constructs (Extended Data Fig. 5k).

Cells devoid of TREX1 display cytoplasmic L1 DNA, accumulation of which can be inhibited with NRTIs[11]. While lack of BrdU incorporation is a canonical feature of senescent cells (Extended Data Fig. 1b), longer term labeling revealed DNA that was predominantly cytoplasmic and highly enriched for L1 sequences (Extended Data Fig. 6a, b). The synthesis of cytoplasmic L1 DNA could be almost completely blocked with the NRTI lamivudine (3TC) or shRNA to L1 (Fig. 3a, c). An antibody to DNA:RNA hybrids detected a cytoplasmic signal in senescent cells that largely colocalized with ORF1 protein and turned into a ssDNA signal following RNase digestion (Extended Data Fig. 6c). Analysis of BrdU-labeled L1 sequences in senescent cells showed them to be localized throughout the L1 element (Extended Data Fig. 6d, e). A relative increase of L1HS sequences in total cellular DNA can also be detected by a qPCR assay[6,16]. 3TC in the range of 7.5–10 μM completely blocked this increase in senescent cells and also quenched the activity of a L1 retrotransposition reporter (Extended Data Fig. 5d, e).

L1 knockdown with shRNA or treatment of cells with 3TC significantly reduced interferon levels, as well as reducing the IFN-I response more broadly in both late senescent and 3X cells (Fig. 3b, Extended Data Fig. 7a). 3TC in the range of 7.5–10 μM optimally inhibited the IFN-I response, and was the most effective of 4 NRTIs tested (Extended Data Fig. 5f, j). The relative efficacies of the NRTIs are consistent with their ability to inhibit human L1 RT[15]. 3TC also antagonized the IFN-I response in other forms of senescence, OIS and SIPS (Fig. 3e).

We passaged cells in the continuous presence of 3TC from the proliferative phase into deep senescence. 3TC did not significantly affect the timing of entry into senescence, induction of p21 or p16, or the early SASP response (such as upregulation of IL-β) (Fig. 3f, Extended Data Fig. 7b). However, the magnitude of the later SASP response (such as induction of CCL2, IL-6 and MMP3) was significantly dampened. Treatment with L1 shRNA also reduced the expression levels of IL-6 and MMP3 in late senescent cells (Extended Data Fig. 6f). Hence, while L1 activation and the ensuing IFN-I response are relatively late in onset, they contribute importantly to the mature SASP and proinflammatory phenotype of senescent cells.

3TC did not affect L1 transcript levels (Extended Data Fig. 5i), suggesting that the INF-I response is triggered by L1 cDNA. As this model would predict, knockdown of the cytosolic DNA sensing pathway components cGAS or STING[17] inhibited the IFN-I response in both late senescent and 3X cells (Extended Data Fig. 5l and Fig. 7c, d), and also downregulated the SASP response in late senescent cells (Extended Data Fig. 7e).

NRTIs alkyl-modified at the 5' ribose position cannot be phosphorylated and hence do not inhibit RT enzymes; however, they possess intrinsic anti-inflammatory activity by inhibiting P2X7-mediated events that activate the NLRP3 inflammasome pathway[18]. Tri-methoxy-3TC (K-9), at 10 μM or 100 μM, did not inhibit the IFN-I response in either late senescent or 3X cells (Extended Data Fig. 7f). Hence, the effect of 3TC on the IFN-I pathway requires RT inhibition. At high concentrations (100 μM) K-9 had some inhibitory activity on markers of inflammation, as reported[18] (Extended Data Fig. 7g).

To test the role of interferon signaling in SASP we inactivated the IFN-α/β receptors (IFNAR1 and 2) using CRISPR/Cas9. Effective ablation of IFN-I signaling was achieved in both early passage and deep senescent cells (Extended Data Fig. 5m). In both replicative and SIPS forms of senescence, loss of interferon signaling antagonized late (CCL2, IL-6, MMP3) but not early (IL-1β) SASP markers (Fig. 3d). This further demonstrates that IFN-I signaling contributes to the establishment of a full and mature SASP response in senescent cells.

## Activation of L1 in human and mouse tissues

Activation of L1 expression in human cancers has been detected with an ORF1 antibody[4]. The same reagent showed widespread ORF1 expression in both senescent and 3X cells (Extended Data Fig. 8a, c, f). In skin biopsies of normal aged human individuals, we found that 10.7% of dermal fibroblasts were positive for the senescence marker p16, which is in the range documented in aging primates[19] (Extended Data Fig. 8b, d, f, h). Some of the p16 positive dermal fibroblasts were also positive for ORF1 (10.3%). Notably, we never observed ORF1 in the absence of p16 expression. We also detected, at the single cell level, the presence of phosphorylated STAT1, consistent with the presence of interferon signaling in the tissue microenvironment[20] (Extended Data Fig. 8b, e, g). Hence, a fraction of senescent cells in normal human individuals display activation of L1, consistent with these events accumulating during the progression of senescence.

We next examined mice and found that L1 mRNA was progressively upregulated with age in several tissues (Extended Data Fig. 10g). The detected L1 RNA sequences were predominantly sense strand, represented throughout the element, and all three active L1 families were detectable (Extended Data Fig. 6g, h). At the protein level, the frequency of L1 Orf1 positive cells increased in tissues with age (Fig. 4a). Regions of Orf1 staining colocalized with senescence-associated β-galactosidase (SA-β-Gal) activity (Fig. 4b). Notably, we found that several IFN-I response genes (Ifn-α, Irf7, Oas1) as well as pro-inflammatory and SASP markers (Il-6, Mmp3, Pai1) were upregulated in tissues of old mice (Fig. 4c, Extended Data Fig. 9). We also observed an increase in L1 expression and IFN-I

response genes (Ifn-α, Oas1) in an experimentally induced model of cellular senescence (young animals subjected to sublethal irradiation; Fig. 4d).

We treated old animals (26 months) for two-weeks with 3TC (administered in water at human therapeutic doses) and found a broad and significant downregulation the IFN-I response and alleviation of the SASP pro-inflammatory state (Fig. 4c, for the full dataset see Extended Data Fig. 9 and Supplementary Table 7). Expression of L1 mRNA and p16 was weakly downregulated, but in most cases did not reach statistical significance. K-9 did not affect either the IFN-I or SASP responses. Immunofluorescence analysis of tissue sections confirmed that senescent cells expressed SASP, and Orf1-expressing cells activated IFN-I signaling (Extended Data Fig. 10a-c). Treatment with 3TC significantly reduced both IFN-I and SASP, but not L1 expression or the presence of senescent cells. Hence, NRTIs can be categorized as “senostatic” agents, to contrast them from “senolytic” treatments that remove senescent cells from tissues[21,22].

Decreased adipogenesis[23] and thermogenesis[24] are features of natural aging and both were increased in old animals by 2 weeks of 3TC treatment (Extended Data Fig. 10d-f). Longer term treatments (from 20 to 26 months of age) were effective at opposing several known phenotypes of aging: macrophage infiltration of tissues, a hallmark of chronic inflammation[23,25], glomerulosclerosis of the kidney[26] and skeletal muscle atrophy[27] (Fig. 4e). Macrophage infiltration of white adipose was especially responsive, returning to youthful (5 month) levels with only 2 weeks of 3TC.

The activation of endogenous L1 elements and the ensuing robust activation of an IFN-I response is a novel phenotype of senescent cells, including naturally occurring senescent cells in tissues. This phenotype evolves progressively during the senescence response and appears to be an important, but hitherto unappreciated component of SASP. We show that the expression of three regulators, RB1, FOXA1 and TREX1 changes during senescence, and that these changes are both sufficient and necessary to allow the transcriptional activation of L1s (Fig. 4g). Hence, multiple surveillance mechanisms need to be defeated to unleash L1, which underscores the importance of keeping these elements repressed in somatic cells. We anticipate that future work will uncover additional mechanisms and failure points that can lead to the activation of endogenous RTEs.

Activation of innate immune signaling in response to L1 activation during cellular senescence and aging proceeds through the interferon-stimulatory DNA (ISD) pathway. Cytoplasmic DNA can originate from several sources, such as mtDNA released from stressed mitochondria[28] or cytoplasmic chromatin fragments (CCF) released from damaged nuclei[29,30]. Our results suggest that L1 cDNA is an important inducer of IFN-I in senescent cells. Remarkably, NRTI treatment effectively antagonized not only the IFN-I response but also more broadly reduced age-associated chronic inflammation in multiple tissues. Given

Sterile inflammation, also known as inflammaging, is a hallmark of aging and a contributing factor to many age-related diseases[31,32]. We propose that activation of L1 elements (and possibly other RTEs in the mouse) promotes inflammaging, and that the L1 RT is a relevant target for the development of drugs to treat age-associated disorders.

# METHODS

## Cell culture.

Several different strains of normal human fibroblasts were employed in this study. LF1 cells were derived from embryonic lung tissue as described[33]. These cells have been in continuous use in our laboratory since their isolation in 1996. For this study original samples frozen in 1996 and in continuous storage in our laboratory were recovered and used. IMR-90 and WI-38 cells were obtained from the ATCC. None of these cell lines are listed in the International Cell Line Authentication Committee (ICLAC) database. These normal fibroblast cell lines were cultured using physiological oxygen conditions (92.5% $N_2$, 5% $CO_2$, 2.5% $O_2$), in Ham's F-10 nutrient mixture (Thermo Scientific) with 15% fetal bovine serum (FBS, Hyclone). Medium was additionally supplemented with L-glutamine (2 mM), penicillin and streptomycin[34]. Cell cultures were periodically tested for mycoplasma contamination with MycoAlert ® Mycoplasma Detection Kit (Lonza).

To obtain replicatively senescent (RS) cells, LF1 cultures were serially propagated until proliferation ceased. At each passage, after reaching 80% confluence cells were trypsinized and diluted 1:4. Hence each passage is equivalent to approximately 2 population doublings. In early passage cultures the time between passages is constant at approximately 3 days. As cultures approached senescence the time between passages gradually increased. An interval of 2–3 weeks indicated that the culture was in its penultimate passage. At this point, after reaching 80% confluence, the cells were replated at 1:2 dilution, and this time was designated as the last passage (point A in Extended Data Fig. 1a). Some cell growth typically does occur in the next 2–3 weeks, but the cultures do not reach 80%. Under this experimental regimen the majority of the cells in the culture enter senescence within a 3–4 weeks window centered roughly around the time of last passage (grey bar in Extended Data Fig. 1a). At point B (4 weeks) the cultures were trypsinized and replated as described[35] to eliminate a small fraction of persisting contact-inhibited cells. Cultures were again replated at point C (8 weeks).

Oncogene-induced senescence (OIS) was elicited by infecting proliferating LF1cells with pLenti CMV RasV12 Neo (gift from Eric Campeau, Addgene plasmid # 22259). Generation of lentiviral particles and the infection procedure are described below. At the end of the infection cells were reseeded at 15–20% confluency and selected with G418 (250 μg/ml) maintained continuously until the end of the experiment Medium was changed every 3 days until the cultures were harvested at the indicated time points. Stress-induced premature senescence (SIPS) was elicited by X-ray irradiation with 20 Gy given at a rate of 87 cGy/min in one fraction using a cesium-137 gamma source (Nordion Gammacell 40). Cells were 15–20% confluent at the time of irradiation. Medium was changed immediately after irradiation, and at 3 day intervals thereafter. 293T cells (Clontech) were used to package lentivirus vectors and were cultured at 37°C in DMEM with 10% FBS under normoxic conditions (air supplemented with 5% $CO_2$).

### Nucleoside reverse transcriptase inhibitors.

All NRTIs (lamivudine, 3TC; zidovudine, AZT; abacavir, ABC; emtricitabine, FTC) used in this study were USP grade and obtained from Aurobindo Pharma, Hyderabad, India. For Trizivir (TZV), its constituents (ABC, AZT and 3TC) were combined in the appropriate amounts. Kamuvudine-9 (K-9)[36] was provided by Inflammasome Therapeutics.

### Mouse husbandry.

Compliance with relevant ethical regulations and all animal procedures were reviewed and approved by the Brown University Institutional Animal Care and Use Committee. C57BL/6J mice of both sexes were obtained from the NIA Aged Rodent Colonies (www.nia.nih.gov/research/dab/aged-rodent-colonies-handbook) at 5 and 18 months of age. The 5 month old animals were sacrificed after a short (1 week) acclimatization period, a variety of tissues were harvested, snap frozen in $LN_2$ and stored at −80°C. The 18 month old animals were housed until they reached a desired age. Mice were housed in a specific pathogen-free AAALAC-certified barrier facility. All procedures were approved by the Brown University IACUC committee. Cages, bedding (Sani-chip hardwood bedding) and food (Purina Lab Chow 5010) were sterilized by autoclaving. Food and water (also sterilized) were provided *ad libitum*. A light-dark cycle of 12 hours was used (7 AM On, 7 PM Off). Temperature was maintained at 70°F, and humidity at 50%. All animals were observed daily and weighed once per week. In a pilot experiment 3 cohorts of 10 animals each were treated with 3TC dissolved in drinking water (1.5 mg/ml, 2.0 mg/ml, 2.5 mg/ml) continuously from 18 months until sacrifice at 24 months. The fourth (control) cohort was provided with the same water without drug. No significant differences in behavior, weight, or survival were observed between the 4 cohorts during the entire experiment. Once during the experiment (at 20 months of age) the animals were subjected to a single tail bleed of approximately 70 μl. The collected plasma was shipped to the University of North Carolina CFAR Clinical Pharmacology and Analytical Chemistry Core for analysis of 3TC. For the 2 mg/ml cohort the concentration of 3TC in plasma averaged 7.2 μM. This dose of drug was chosen for further experiments to mimic the human HIV therapeutic dose (300 mg per day, 5–8 μM in plasma)[37]. For the experiments presented in this communication animals were aged in house until they reached 26 months of age. They were then assigned randomly to two cohorts by a technician that was blinded to the appearance or other characteristics of the animals. One cohort was treated for 2 weeks with 2 mg/ml of 3TC in drinking water, and the other (control) cohort with same water without drug, administered in the same manner. At the end of the treatment period all animals were sacrificed and harvested for tissues as described above. All the animals in both cohorts were all included in all subsequent analyses. The experiment was performed on separate occasions with male and female animals. Non-lethal total body irradiation (6 Gy) was performed by the group of Christian Beauséjour as described[38] and tissue specimens were shipped to Brown University on dry ice.

### PCR.

The ABI ViiA 7 instrument (Applied Biosystems) was used for all experiments. qPCR of DNA was performed using the Taqman system (Applied Biosystems) as described by Coufal *et al.* (2009)[16]. 100 pg of purified genomic DNA was used with the indicated primers

(Supplementary Table 1). Reverse transcription qPCR (RT-qPCR) of RNA was performed using the SYBR Green system (Applied Biosystems). Polyadenylated RNA was used in all experiments assessing transcription of L1 elements, and total RNA was used for all other genes. Total RNA was harvested using the Trizol reagent (Invitrogen). Poly(A) RNA was isolated from total RNA using the NEBNext Poly(A) mRNA Magnetic Isolation Module (New England Biolabs). 1 μg of total RNA, or 10 ng of poly(A) RNA, were reverse-transcribed into cDNA in 50 μl reactions using the Taqman kit (Applied Biosystems). To assess strand-specific transcription, the random primers in the RT reaction were substituted with a strand-specific primer to the target RNA. 1 μl of each RT reaction was used in subsequent qPCR reactions. GAPDH was used as the normalization control in experiments with human cells. The arithmetic mean of Gapdh and two additional controls (Hsp90 and GusB) was used for normalization of RT-qPCR experiments with murine tissues, with the exception of liver that was normalized to Hsp90 and GusB. For measuring L1 transcription, poly(A) RNA samples were exhaustively digested with RNase-free DNase (Qiagen) prior to the synthesis of cDNA[6]. Effectiveness of the DNase digestion was assessed using controls that omitted the RT enzyme.

### Design of PCR primers.

Primer sets 1 to 5 (Supplementary Table 1, amplicons A to E in Fig. 1b) to human L1 were designed to preferentially amplify elements of the human-specific L1HS and evolutionarily recent primate-specific L1PA(2–6) subfamilies, as follows. First, the consensus sequences of L1HS and L1PA2 through L1PA6 elements were obtained from Repbase (Genetic Information Research Institute, http://www.girinst.org/repbase/update/browse.php). Second, a consensus sequence of these 6 sequences was generated with the Clustal Omega multiple sequence alignment tool (http://www.ebi.ac.uk/Tools/msa/clustalo/)[39]. Primer design was then done on the overall consensus with Primer3 and BLAST using the NCBI Primer-BLAST tool (http://www.ncbi.nlm.nih.gov/primer-blast/)[40]. L1 primer pairs were evaluated for their targets using the *In-Silico* PCR (https://genome.ucsc.edu/cgi-bin/hgPcr) tool against the latest genome assembly (hg38) with a minimum perfect match on 3' end of each primer equal to 15. Primers to ORF2 (primer set 6, amplicon F in Fig. 1b) were developed by Coufal et al. (2009)[16] to preferentially target L1HS. Primers to assess transcription of active murine L1 elements (primer set 37, Supplementary Table 1) were designed on the combined consensus sequence of the L1MdA and L1Tf families obtained from Repbase and validated as described above. L1 primer pairs spanning the full length these elements (primer sets 48–50) were designed using the same strategy. Primer pairs specific to the three active families of murine L1 elements (primer sets 51–53) were designed exploiting polymorphisms in the 5'UTR region. RT-qPCR analysis of L1 transcription was performed on poly(A) purified RNA using the SYBR Green method. For all other (non-L1) genes, whenever possible, primers are separated by at least one intron in the genomic DNA sequence (as indicated in Supplementary Table 1). Primers to the human IFN alpha family were designed against a consensus sequence of all the human IFN alpha gene sequences (IFNA1, IFNA2, IFNA4, IFNA5, IFNA6, IFNA7, IFNA8, IFNA10, IFNA13, IFNA14, IFNA16, IFNA17, IFNA21) generated with the Clustal Omega multiple sequence alignment tool. All primers against murine targets were designed as described above and are listed in Supplementary Table 1. Sequences of primers corresponding to a consensus of all the murine IFN alpha genes, as

well as to the IFNB1 gene, were obtained from the publication by Gautier et al.[41]. For quantifying relative L1 genomic copy number (human cells) we used the TaqMan multiplex method developed by Coufal et al. (2009)[16]. These primers are listed as set #6 and set #7 (with their corresponding VIC and 6FAM probes) in Supplementary Table 1.

### Chromatin Immunoprecipitation.

All ChIP experiments were performed using the Chromatrap spin column ChIP kit (Porvair). Briefly, $2\times10^6$ cells were crosslinked in their culture dishes with 1% formaldehyde (10 min., room temperature), quenched with glycine, washed twice with ice-cold PBS (containing protease inhibitors), and finally scraped into a microfuge tube. Cell pellets were resuspended in 0.4 ml of hypotonic buffer and incubated for 10 min. on ice. Nuclei were spun down, resuspended in 0.3 ml lysis buffer, and sonicated using a Bioruptor UCD-200 instrument (Diagenode) set to pulse on high (30 sec. followed by 30 sec. rest) for a total time of 10 min. The extracts were centrifuged in a microfuge (top speed, 5 min., 4°C) to remove debris, the supernatants were transferred to new tubes, and stored at −80°C. An amount of extract containing 2 μg of DNA was combined with 4 μg of antibody and loaded on a Chromatrap solid phase Protein A matrix. Immunocomplexes were allowed to form overnight at 4˚C with mild agitation, following which the samples were washed and eluted according to the manufacturer's protocol. Rabbit IgG and 1% input were used as controls. 1 μl of immunoprecipitated DNA was used in each qPCR reaction.

### BrdU pull-down.

To obtain quiescent cells, proliferating cells were grown to 50% confluence, serum supplementation of the medium was changed to 0.1% FBS, and incubation was continued until harvest. Quiescent and senescent cells were continuously labeled for two weeks with BrdU (BrdU Labeling Reagent, Thermo Fisher) according to the manufacturer's protocol for labeling of culture cells. Cell were harvested and counted: $5\times10^5$ cells were processed per condition. Genomic DNA was purified via Phenol:Chloroform extraction, RNase A treated and subsequently sheared using a Bioruptor UCD-200 instrument (pulse on Low, 30 seconds on and 30 seconds off, 10 minutes total). DNA tubes were incubated in a heat block (100°C) for exactly one minute and then flash frozen in liquid nitrogen. Tubes were let thaw at room temperature and 1 μg of purified anti-BrdU antibody (BD Pharmingen, Cat. # 555627) was added per tube together with magnetic protein A/G beads and ChIP Dilution Buffer. Immuno-slurries were incubated overnight at 4°C with constant rotation. Immuno-captured BrdU labeled DNA was purified according to the Magna ChIP™ A/G Chromatin Immunoprecipitation Kit (Millipore Sigma). Unbound DNA was kept as input. 1 μl of immunoprecipitated DNA was used in each qPCR reaction. Alternatively, to enrich for single-stranded BrdU-labeled DNA the heat-mediated denaturation was omitted and samples were processed for BrdU pull-down as above. The DNA second strand was then generated by adding a mixture of random primers (Thermo Fisher), second strand synthesis reaction buffer, dNTPs and DNA Pol I (New England Biolabs). The reaction was incubated for 4 hrs. at 16˚C and subsequently purified by phenol-chloroform extraction. Following the second strand synthesis, the dsDNA was end-repaired with the End-It DNA End-Repair Kit (Epicenter, Cat. #ER0720). Blunt-ended fragments were cloned using the Zero Blunt TOPO PCR Cloning Kit (Thermo Fisher), and then used to transform One Shot TOP10 chemically

competent *E. coli* (Thermo Fisher, Cat. # C404010). Individual colonies were picked and subjected to Sanger sequencing using a T7 promoter primer at Beckman Coulter Genomics.

### RNA-seq.

Total RNA from early passage, early and deep senescent cells (Extended Data Fig. 1a) was extracted as described above. The total RNA was processed with the Illumina TruSeq Stranded Total RNA Ribo-Zero kit and subjected to Illumina HiSeq2500 2×125bp paired end sequencing using v4 chemistry at Beckman Coulter Genomics Inc. Over 70 million reads were obtained for each sample. The RNA-seq experiment was performed in three biological replicates.

Raw RNA-sequencing reads were aligned to the GrCh38 build of the human genome using HiSat2[42]. Counts mapping to the genome were determined using featureCounts[43]. Counts were then normalized using the trimmed mean of M-values (TMM) method in EdgeR[44]. EdgeR was additionally used to derive differential expression from the normalized data set. Differential expression data were then ranked by $\log_2$ fold change and input into the GenePattern interface for GSEA Preranked, using 1000 permutations, to determine enrichment for KEGG pathways, SASP, and the interferon response[45,46]. The outputs were then corrected for multiple comparisons by adjusting the nominal p value using Benjamini-Hochberg method[47]. Data were displayed using GENE-E software (http://www.broadinstitute.org/cancer/software/GENE-E).

### In silico analysis of transcription factors binding to L1.

Transcription factor profiles were created using ChIP-seq data from the ENCODE project (GEO accession numbers GSE2961 and GSE32465). Transcription factor ChIP-seq and input control reads were aligned to the consensus sequence of L1HS using bowtie1[48]. The log2 fold change enrichment was calculated per base pair of the L1HS consensus using the transcription factor ChIP-seq read coverage per million mapping reads (RPM) versus input control RPM values, and smoothed by LOESS smoothing with a parameter $\alpha$=0.1. The total number of mapping reads used in RPM normalization was determined from a separate bowtie1 alignment to the human genome (hg19).

### Construction of FOXA1 reporters.

L1 promoter reporter plasmids L1WT and L1 del (390–526) were obtained from Sergey Dmitriev, Institute of Bioorganic Chemistry, Moscow[49,50]. Both contain luciferase as the reporter cloned in the sense orientation. To determine antisense transcription from the same plasmid EYFP was inserted in the inverse orientation upstream of the L1 5' UTR as follows. The EYFP sequence was excised from pEYFP-N1 (Clontech, Cat. # 6006–1) with AgeI and NotI and blunt ended. Plasmids L1WT and L1del were digested with XbaI, blunted and treated with FastAP (Fermentas). Successful insertion of anti-sense EYFP was verified using PCR primers AAAGTTTCTTATGGCCGGGC (in EYFP) and GCTGAACTTGTGGCCGTTTA (in L1 promoter) and Sanger sequencing. Plasmid pcDNA3.1/LacZ was used as the co-transfection control. Luciferase and β-galactosidase assays were performed as described[49]. EYFP-N1 was used as a positive control for detecting

the EYFP signal. Co-transfections were performed on early passage LF1 cells using Lipofectamine with Plus Reagent (Invitrogen) according to the manufacturer's instructions.

### Lentiviral vectors.

Constructs were obtained from public depositories as indicated below. Virions were produced and target cells were infected as described (https://www.addgene.org/tools/protocols/plko/). shRNA sequences were obtained from The RNAi Consortium (TRC, http://www.broad.mit.edu/genome_bio/trc/rnai.html), cloned into third generation pLKO.1 vectors and tested for efficacy. Four selectable markers were used to allow multiple drug selections: pLKO.1 puro (2 μg/ml) and pLKO.1 hygro (200 μg/ml) (gifts from Bob Weinberg, Addgene plasmid # 8453, 24150), pLKO.1 blast (5 μg/ml) (gift from Keith Mostov, Addgene plasmid # 26655), pLKO.1 neo (250 μg/ml) (gift from Sheila Stewart, Addgene plasmid 13425). pLKO-RB1-shRNA63 and pLKO-RB1-shRNA19 were a gift from Todd Waldman (Addgene plasmids # 25641 and 25640)[51]. For FOXA1 shRNAs TRCN0000014881 (a) and TRCN0000014882 (b) were used. For TREX1 shRNAs TRCN0000007902 (a) and TRCN0000011206 (b) were used. For knockdown of L1 we designed and tested 9 shRNAs, of which two (shL1_11 to ORF1, AAGACACATGCACACGTATGT, and shL1_44 to ORF2 AAGACACATGCACACGTATGT) showed significant knockdown (Extended Data Fig. 5g) and were chosen for further work. The remaining 7 shRNAs produced no or minimal knockdown. For cGAS shRNAs TRCN0000128706 (a) and TRCN0000128310 (b) were used. For STING shRNAs TRCN0000161345 (a) and TRCN0000135555 (b) were used.

All ectopic expression experiments used constructs generated by the ORFeome Collaboration (http://www.orfeomecollaboration.org/) in the lentivirus vector pLX304 (blasticidin resistant, Addgene plasmid 25890) and were obtained from the DNASU plasmid repository (https://dnasu.org/DNASU/Home.do): RB1 (ccsbBroad304_06846, HsCD00434323), TREX1 (ccsbBroad304_02667, HsCD00445909), FOXA1 (ccsbBroad304_06385, HsCD00441689).

All the interventions in senescent cells were initiated by infecting cells at 12 weeks of senescence (point D in Extended Data Fig. 1a). Following appropriate drug selections cells were incubated until 16 weeks of senescence (point E in Extended Data Fig. 1a), when they were harvested for further analysis.

The 3X intervention was performed by infecting early passage LF1 cells sequentially with vectors pLKO.1 puro shRB, pLKO.1 hygro shTREX1 and pLX304 blast FOXA1 (Extended Data Fig. 5c). After each infection the arising drug resistant pool of cells was immediately infected with the next vector. After the third infection the cells were harvested for further analysis 48 hours after the drug selection was complete. The infections were also performed in various combinations and in each case resulted in the activation of L1 expression, entry into senescence, and induction of an IFN-I response. The sequence above was chosen because it gave the most efficient selection of cells for further analysis. To allow an additional (fourth) intervention in 3X cells (shL1, shSTING, or shCGAS), hairpins targeting RB1 were re-cloned in pLKO.1 neo, thus freeing pLKO.1 puro for the fourth gene of interest. This allowed an efficient drug selection process and sample harvest 48 hrs. after the last selection.

### Retrotransposition reporters.

The two-vector dual luciferase reporter system reported by Xie et al. (2011)[52] was adapted for lentiviral delivery. The $L1_{RP}$-Fluc reporters were recloned from plasmids pWA355 and pWA366 into the lentiviral backbone pLX304. pWA355 contains a functional, active $L1_{RP}$ element, whereas pWA366 contains $L1_{RP}$(JM111), a mutated element carrying two missense mutations in ORF1 that is unable to retrotranspose. Early passage LF1 cells were infected with a puromycin resistant lentivirus expressing Rluc. Pooled drug resistant cells were then infected with high titer particles of pLX304-WA355 or pLX304-WA366 constructs. Immediately after infection cells were treated for four days with 3TC (at the indicated concentrations). Cells were then harvested and assayed for Rluc amd Fluc luciferase activities. The native L1 retrotransposition reporter pLD143[53] was co-transfected with pLKO vectors (shLuc, shL1_11 and shL1_44) into HeLa cells using FuGene HD (Promega). Cell culture, transfection and retrotransposition assays were done as described above. Retrotransposition activity was normalized to the activity of $L1_{RP}$ co-transfected with shLuc. Three independent experiments were performed for each construct.

### Identification of expressed L1 elements by long-range RT-PCR and 5’RACE.

Total RNA was harvested from cells using the Trizol reagent (Invitrogen). The RNA was further purified using the Purelink RNA Mini kit (Invitrogen) with DNase I digestion. From the eluted total RNA, poly(A) RNA was isolated using the NEBNext Poly(A) mRNA Magnetic Isolation Module (New England Biolabs). The forward primer (MDL15UTRPRAF, primer set 1, Supplementary Table 1) was used with either of two reverse primers (MDL15UTRPRCR, primer set 3, amplicon size 537 bp) or MDL15UTRPRDR, primer set 4, amplicon size 654 bp). A high-fidelity thermostable reverse transcriptase (PyroScript RT-PCR Master Mix Kit, Lucigen) was used with 10 ng of poly(A) mRNA per reaction and amplified for 10 cycles. No template and RNaseA treated samples were used as negative controls. The generated amplicons were cloned into the TOPO-TA (Invitrogen) vector and the resulting plasmids were used to transform One Shot TOP10 chemically competent *E. coli*. Individual colonies were picked and subjected to Sanger sequencing using a T7 promoter sequencing primer at Beckman Coulter Genomics. 96 sequencing reactions (1 plate) were performed for each primer pair in four experiments for a total of 768 sequenced clones. Sequencing data were trimmed to remove the RT-PCR primers and BLASTed against the human genome (GRCh38) with a match/mismatch cost of +1, −4 and allowing species-specific repeats for Homo sapiens. Only perfect hits were scored and annotated for genomic coordinates. 658 clones could be mapped to the reference genome, 51 contained at least 1 mismatch and thus likely represent elements that are polymorphic in the cell line, and 58 were cloning artifacts. Whenever a clone presented multiple instances of perfect identity a fractional count was adopted, dividing the counts by the number of elements sharing the same sequence. Each mappable clone was further analyzed using L1Xplorer[54] to recover the classification features of the L1 element and whether it is intact.

Alternatively, poly(A) RNA isolated as above was subjected to Rapid Amplification of cDNA Ends (RACE). Each reaction contained 10 ng of poly(A) RNA and was processed using the 5’RACE System kit (Thermo Fisher, Cat. # 18374–041). The two antisense gene-

specific primers (GSP) used for 5'RACE were: for GSP1, MDL15UTRPRDR (primer set 4, Supplementary Table 1), and for the nested GSP2, MDL15UTRPRCR (primer set 3, Supplementary Table 1). Amplification products were cloned and sequenced as above, using a T7 promoter sequencing primer by Beckman Coulter Genomics. A total of 94 clones were sequenced; 26 contained mostly a polyG stretch generated by the tailing step in the RACE protocol and 18 could not be mapped to the human genome. The remaining 50 mappable clones contained L1 sequences and were aligned to the L1HS consensus using a setting of >95% identity at positions 1–450 (http://www.girinst.org/repbase/update/browse.php). The mappable clones were also assigned to individual L1 families using RepEnrich software[55]. Pairwise alignments to the consensus were performed with LALIGN[56]. Multiple sequence alignments were calculated using MAFFT (Multiple Alignment using Fast Fourier Transform) with the L-INS-i algorithm (accurate for alignments of <200 sequences)[57]. Alignment visualization, %-identity coloring and consensus were generated by Jalview[58].

### Generation and analysis of CRISPR-Cas9 knockouts.

Three distinct gRNA sequences for each chain of the IFNAR receptor (IFNAR1 and IFNAR2), listed in the GeCKO v2.0 resource (Feng Zhang Lab, MIT, http://genome-engineering.org/gecko/?page_id=15)[59], were tested and the following ones were chosen: IFNAR1 (HGLibA_29983) AACAGGAGCGATGAGTCTGTA; IFNAR2 (HGLibA_29985) GTGTATATCAGCCTCGTGTT. Cas9 and gRNAs were delivered using a single lentivirus vector (LentiCRISPR_v2, Feng Zhang Lab, MIT; Addgene plasmid # 52961), carrying a puromycin resistance gene. The efficacy of the CRISPR-Cas9 mutagenesis, on the basis of which the above two gRNAs were chosen, was evaluated by treating the infected and drug-selected cells with interferon (universal type I interferon, PBL Assay Science, Cat. # 11200–1) and monitoring nuclear translocation of phospho-STAT2 and IRF9 by immunofluorescence. The absence of translocation signifies lack of IFN-I responsiveness and hence loss of IFNAR function. Experimental procedures followed the protocols provided by the Zhang lab (http://genome-engineering.org/gecko/wp-content/uploads/2013/12/lentiCRISPRv2-and-lentiGuide-oligo-cloning-protocol.pdf)[60]. In the experiment shown in Fig. 3h (RS) and Extended Data Fig. 5k, both IFNAR1 and IFNAR2 gRNAs were used to treat the same cells to further increase the efficacy of ablating the INF-I response. For early passage and senescent cells co-infections of IFNAR1 and IFNAR2 vectors were performed followed by selection with puromycin. For senescent cells high titer lentivirus particles were applied to senescent cells at 12 weeks in senescence (point D, Extended Data Fig. 1a) and cells were assayed 4 weeks later (point E, Extended Data Fig. 1a). For the experiment shown in Fig. 3h (SIPS), edited early passage cells were single-cell cloned. 24 single cells were isolated using the CellRaft technology (Cell Microsystems) and expanded. Genomic screening of the CRISPR cut site was performed by the CRISPR Sequencing Service (CCIB DNA Core, Massachusetts General Hospital, https://dnacore.mgh.harvard.edu/). The successful knock out of IFNAR1 and IFNAR2 was verified in 4 out of the 24 expanded clonal cell lines.

### Immunoblotting.

Cells were harvested in Laemmli sample buffer (60 mM Tris pH 6.8, 2% SDS, 10% glycerol, 100 mM DTT) and boiled for 5 min. at 100°C. Whole cell extracts (60 μg protein)

were separated by SDS-PAGE and transferred onto Immobilon-FL membranes (Millipore). Nonspecific binding was blocked by incubation in 4% bovine serum albumin (BSA; Thermo Fisher) and 0.1% Tween-20 in PBS for 1 hr. at room temperature. Primary antibodies were diluted in the blocking solution and incubated overnight at 4°C. A list of all the primary antibodies is provided in Supplementary Table 2. Secondary antibodies were diluted in blocking solution and incubated for 1 hr. at room temperature. Signals were detected using the LI-COR Odyssey infrared imaging system (LI-COR Biosciences). For the quantification of signals all samples to be compared were run on the same gel. Loading standards were visualized on the same blot as the test samples using the LI-COR 2-color system. Bands were imaged and quantified using LI-COR software. All bands to be compared were quantified on the same image and were within the linear range of detection of the instrument.

### Immunofluorescence microscopy performed on cells in culture.

Cells were grown on glass cover slips and the samples were processed as previously described[61]. Primary antibodies are listed in Supplementary Table 2. Staining of ssDNA was performed as described by Thomas et al[11]. Briefly, cells seeded on coverslips were fixed on ice with 4% paraformaldehyde (PFA) for 20 min. and then incubated in 100% methanol at −20°C overnight. The cells were then treated with 200 mg/mL RNase A at 37°C for 4 hrs. Cells were blocked with 3% BSA and incubated overnight at 4°C with primary antibodies diluted in 3% BSA. Images were acquired using a Zeiss LSM 710 confocal laser scanning microscope or a Nikon Ti-S inverted fluorescence microscope. All microscope settings were set to collect images below saturation and were kept constant for all images taken in one experiment, as previously described[61]. Image analysis was performed as described below for tissues.

### PCR arrays.

Total RNA was harvested from cells as indicated above (Quantitative PCR) and analyzed using the Qiagen RT² Profiler™ Human Type I Interferon Response PCR Array (Cat. # PAHS-016ZE-4). Reverse transcription reactions were performed with the Qiagen RT$^2$ First Strand Kit (Cat. # 330404) using 1μg of total RNA as starting material. 102 μl of the completed reaction was combined with 650 μl of Qiagen RT² SYBR Green ROX qPCR Mastermix (Cat. # 330521) and 548 μl of RNase-free molecular grade water, and run in the 384-well block on a ViiA 7 Applied Biosystems instrument. All procedures followed the manufacturer's protocols. All conditions were run in triplicate. The results were analyzed using the Qiagen GeneGlobe Data Analysis Center (http://www.qiagen.com/us/shop/genes-and-pathways/data-analysis-center-overview-page/). Briefly, $C_t$ values were normalized to a panel of house keeping genes (HKG). $\Delta C_t$ values ware calculated between a gene of interest (GOI) and the mean HKG value. Fold changes were then calculated using $2^{\wedge}(-\Delta\Delta C_T)$ formula. The lower limit of detection was set at $C_t$ of 35. For any GOI to be considered significant the following filters were set: 1) >2-fold change in expression; 2) p-value >0.05. In addition, genes with an average $C_t > 32$ in both control and test samples were also eliminated.

### Enzyme Linked Immunosorbent Assay (ELISA).

Interferon β levels were quantified with the VeriKine-HS Human IFN Beta Serum ELISA Kit (PBL Assay Science, Cat. # 41415). Cell culture media were conditioned for 48 hrs. before harvest. To remove particles and debris, 1 ml aliquots were spun 5 minutes 5,000 x g. All incubations were performed in a closed chamber at room temperature (22–25ºC) keeping the plate away from temperature fluctuations. 50 µl of sample buffer followed by 50 µl of diluted antibody solution were added to each well. Finally, 50 µl of test samples, standards or blanks were added per well. Plates were sealed and shaken at 450 rpm for 2 hrs. At the end of the incubation period the contents of the plate were removed and the wells were washed three times with 300 µl of diluted wash solution. 100 µl of HRP solution was added to each well and incubated for 30 min. under constant shaking. The wells were emptied and washed four times with wash solution. 100 µl of the TMB substrate solution was added to each well. Plates were incubated in the dark for 30 min. Finally, 100 µl of stop solution was added to each well and within 5 min. absorbance at 450 nm was recorded. The values recorded for the blank controls were subtracted from the standards as well as sample values to eliminate background. Optical densities (OD) units were plotted using a 4-parameter fit for the standard curve and were used to calculate the interferon titers in the samples.

### Human tissue specimens.

We are grateful to Andrea Maier, Mariette Waaijer and Rudi Westendorp for assistance with the human specimens. Human skin specimens were collected as part of the Leiden Longevity Study[62,63] and were provided by P. Eline Slagboom, Leiden University Medical Centre, Netherlands. Informed consent was obtained and all protocols were approved by the ethical committee of the Leiden University Medical Centre. The samples were collected as 4 mm thickness full depth punch biopsies, embedded in optimal cutting compound (OCT), flash frozen, and stored at −80°C. Samples were shipped on dry ice to Brown University. The Brown investigators were blinded to everything except the age and sex of the subjects. The OCT-embedded specimens were cryosectioned at 8 µm thickness using a Leica CM3050S cryomicrotome. The slides were fixed with 4% PFA and 0.5% Triton X-100 in PBS (prewarmed to 37 °C) for 20 min. at room temperature. No further permeabilization was performed. Antibody incubation was preceded by a blocking step with 4% bovine serum albumin (BSA; fraction V, Thermo Fisher), 2% donkey serum, 2% rabbit serum and 0.1% Triton X-100 in PBS for 1 hr. at room temperature. Primary antibodies were diluted in the above blocking solution (1:200) and incubated overnight at 4 °C with rocking in a humidified chamber. The secondary antibodies (AlexaFluor 546 and AlexaFluor 647, Life Technologies) were also diluted in blocking solution and incubated for 2 hrs. at room temperature. Three 15 min. washing steps in PBS, containing 0.2% Triton X-100, followed each antibody incubation. Nuclei were counterstained with 2 µg/ml DAPI in PBS, containing 0.2% Triton X-100, for 15 min. Stained slides were mounted with ProLong Antifade Mountant without DAPI (Life Technologies) and imaged on a Zeiss LSM 710 Confocal Laser Scanning Microscope. A z-series encompassing the full thickness of the tissue was collected for each field. All microscope settings and exposure times were set to collect images below saturation and were kept constant for all images taken in one experiment. Image analysis was performed using either CellProfiler software[64], or ImageJ open source software from the NIH (http://rsbweb.nih.gov/ij/). Nuclei were defined using the DAPI

channel. Cell outlines were defined by radially expanding the nuclear mask using the function *Propagate* until an intensity threshold in the AlexaFluor 546 and AlexaFluor 647 channels was reached. The fluorescence intensity within these regions was then recorded in both channels. For each sample a total of 200 nuclei were recorded in multiple fields. Mouse tissue sections were processed and analyzed in the same way as described above.

### Mouse tissue specimens.

Total RNA was extracted from 50 mg of visceral adipose, small intestine, skeletal muscle, brown adipose or liver tissue by mincing followed by homogenization in Trizol (Invitrogen) using a Power Gen 125 homogenizer (Fischer Scientific). After phase separation, the RNA in the aqueous layer was purified using the Purelink RNA Mini kit (Invitrogen) with DNase I digestion. To assess gene expression by RT-qPCR 1 μg of total RNA was reverse transcribed as described above. In each individual experiment all samples were processed in parallel and no blinding was introduced.

Imaging of whole-mount white adipose tissue followed the method described by Martinez-Santibañez et al. (2014)[65]. Briefly, white adipose tissue (visceral depot) were subdivided into 0.5–1 $cm^3$ sized pieces and incubated in 10 ml of fresh fixing buffer (1% PFA in PBS pH 7.4) for 30 min. at room temperature with gentle rocking. After three washing steps with PBS, the tissue blocks were cut in six equal pieces. All subsequent incubations were performed in 2 ml cylindrical microcentrifuge tubes. Primary antibody incubation was preceded by a blocking step with 5% BSA, 0.1% Saponin in PBS for 30 min. at room temperature. Primary antibodies were diluted in the above blocking solution (1:200) and incubated overnight at 4 °C with gentle rocking. The secondary antibodies (AlexaFluor 546, AlexaFluor 594 and AlexaFluor 647, Life Technologies) were also diluted in blocking solution and incubated for 2 hrs. at room temperature. Three 10 min. washing steps in PBS followed each antibody incubation. Antibody-independent staining of nuclei and lipids was performed after immuno-staining: DAPI and BODIPY (Thermo Fisher) were diluted in PBS with 5% BSA and incubated with tissue specimens for 20 min. followed by three washing steps as above. Stained samples were carefully placed on confocal-imaging optimized #1.5 borosilicate glass chamber slides. A small drop of PBS prevented drying. Acquired images were analyzed as described above.

Co-staining of SA-β-Gal activity and ORF1 protein in liver sections was performed by staining for SA-β-Gal first as described[66]. Subsequently, samples underwent heat-induced epitope retrieval by steaming for 20 min. in antigen retrieval buffer (10 mM Tris, 1 mM EDTA, 0.05% Tween 20, pH 9.0). Samples were then processed for immunofluorescence staining as above (Human tissue specimens).

Kidney tissue preserved in OCT was cryosectioned, treated for 10 min. with 0.5% (w/v) periodic acid, then stained with periodic acid-Schiff's (PAS) reagent (Fisher Scientific, Cat. #SS32–500) for 10 min. Stained tissue sections were mounted with Shandon Aqua Mount (Fisher Scientific, Cat. #14–390-5) and then imaged under bright field illumination. Glomerulosclerosis was scored as described[26]. Briefly, 40 glomeruli per animal were assessed in a blinded fashion and assigned scores of 1–4: score of 1, <25% sclerosis; 2, 25–50% sclerosis; 3, 50–75% sclerosis; 4, >75% sclerosis. The feature used to assess sclerosis

was the strength and pervasiveness of PAS-positive lesions within the glomeruli. As exemplified in Fig. 4e, a sclerotic glomerulus is more shrunken and stains more intensely with PAS.

We thank Darren Baker for guidance with the glomerulosclerosis assay.

Quadriceps muscles were embedded in OCT, sectioned at 12 μm thickness and mounted onto positively charged slides. Sections were stained with H&E (hematoxylin, 3 min. followed by 30 eosin, sec.). Mounted slides were imaged on a Zeiss Axiovert 200M microscope equipped with a Zeiss MRC5 color camera. To measure muscle fiber diameter, the shortest distance across ~100 muscle fibers per animal was measured using ImageJ software as described[27]. The Kolmogorov-Smirnov test was used to assess the statistical significance of the difference between the resulting distributions.

### Statistical treatments.

Excel was used to perform general statistical analyses (means, s.d., t-tests, etc). R software for statistical computing (64-bit version 3.3.2) was used for 1-way ANOVA and Tukey's multiple comparisons post-hoc test. For consistency of comparisons significance in all figures is denoted as follows: $*P < 0.05$, $**P < 0.01$. Sample sizes were based on previously published experiments and previous experience in which differences were observed. No statistical test was used to pre-determine sample size. No samples were excluded. All attempts at replication were successful. There were no findings that were not replicated or could not be reproduced. The nature and numbers of samples analyzed (defined as $n$) in each experiment are listed in the figure legends. The number of independent experiments is also listed in figure legends. The investigators were blinded when quantifying immunofluorescence results. Fields or sections of tissues for quantification were randomly selected and the scored, using methods as indicated for individual experiments. The investigators were also blinded when scoring glomerulosclerosis and muscle fiber diameter. For RNA-seq and PCR array experiments the statistical treatments are described under those sections (above).

## Extended Data

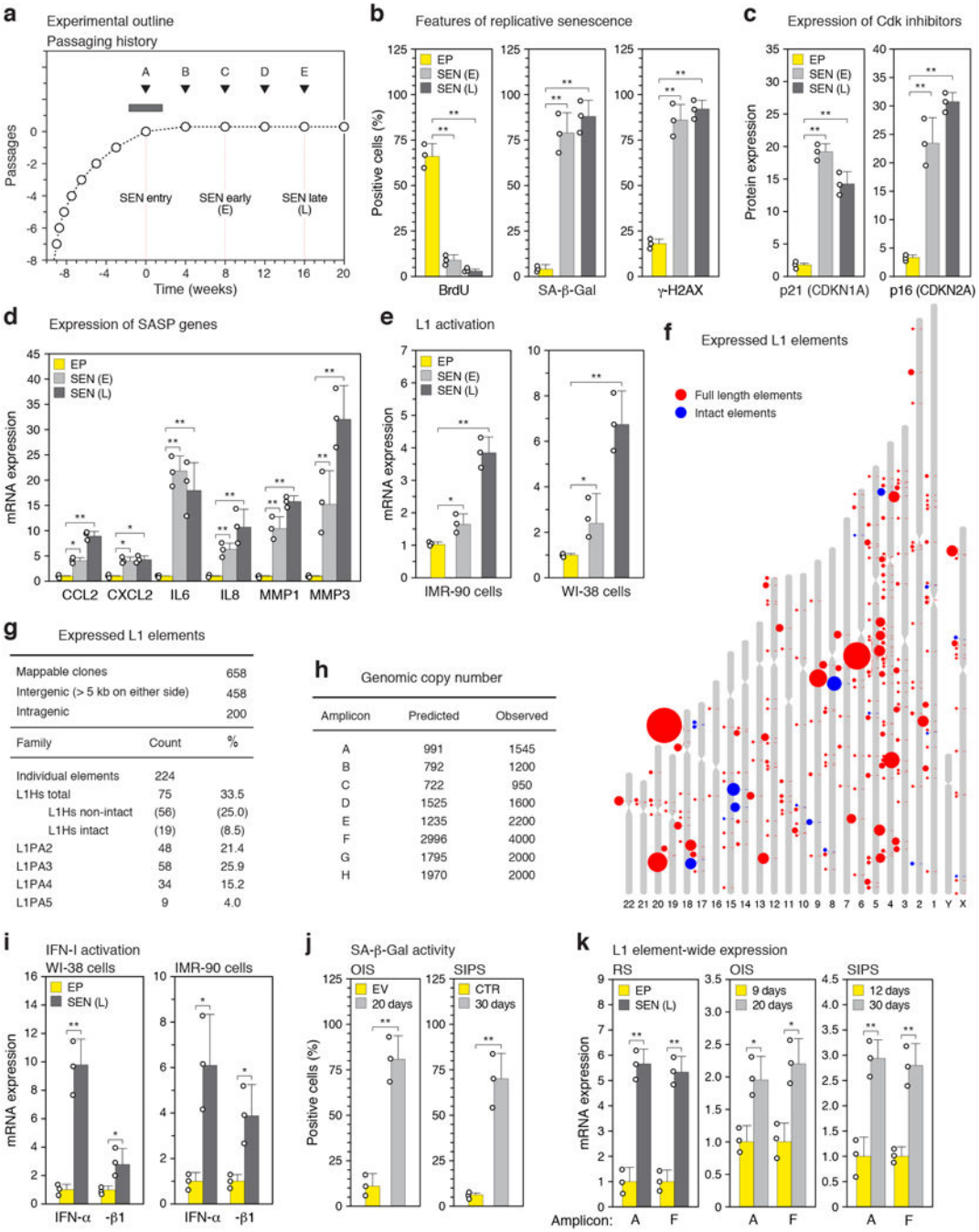


**Extended Data Figure 1. |. Establishment of senescent cultures and analysis of L1 and IFN-I activation.**

**a,** Passaging regimen to obtain long-term replicatively senescent cells (details in Methods). Point A was designated as zero for time in senescence. **b-d,** Confirmation of the senescent status of cultures. A representative experiment is shown; other experiments were monitored in the same manner and generated data that met these benchmarks. EP, early passage control; SEN (E), early senescence (8 weeks); SEN (L), late senescence (16 weeks). **b,** Cells were labeled with BrdU for 6 hours. BrdU incorporation[67] and senescence-associated β-

galactosidase (SA-β-Gal) activity[66] were determined as indicated. DNA damage foci were visualized using γ-H2AX antibodies and immunofluorescence microscopy (IF)[34]. **c**, Expression of p21 (CDKN1A) and p16 (CDKN2A) proteins was determined by immunoblotting. GAPDH was the loading control. For gel source data see Supplementary Fig. 1. **d**, Expression of genes characteristic of the SASP was determined by RT-qPCR. **e,** L1 activation during senescence of IMR-90 and WI-38 strains of fibroblasts was assessed by RT-qPCR using poly(A) purified RNA and primers for amplicon F (Fig. 1b). **f**, Long-range RT-PCR was performed with primers A-forward and C-reverse (amplicon G) and primers A-forward and D-reverse (amplicon H) (Fig. 1b, Supplementary Table 1) and the cDNAs were cloned and sequenced. Several attempts using the same protocol on early passage proliferating cells did not yield any L1 clones. Sequences were mapped to the unmasked reference genome demanding 100% identify. 658 clones could be thus mapped, 51 additional clones contained at least 1 mismatch and thus likely represent elements that are polymorphic in the cell line, and 58 were cloning artifacts. Among the 658 mappable clones 224 unique elements were represented (Supplementary Table 3). Intact elements are the subset of full length elements annotated with no ORF inactivating mutations. Size of the features corresponds to the number of times the element was represented among the 658 clones. **g**, Summary of long-range PCR data presented in (f) and Supplementary Table 3. **h**, Apparent genomic copy numbers of elements detected with our amplicons (see Fig. 1b for locations of amplicons and Methods for primer design strategy). Predicted: *in silico* PCR (Methods). Observed: qPCR was performed on 1 ng of genomic DNA and normalized to a known single copy locus. **i**, Activation of IFN-α and IFN-β1 genes during senescence of WI-38 and IMR-90 cells was determined by RT-qPCR. **j,** Confirmation of the senescent status of cells in OIS (20 days, Fig. 1e) and SIPS (30 days, Fig. 1e) by SA-β-Gal activity. EV, empty vector control; CTR, non-irradiated cells. **k,** Confirmation of full length L1 mRNA expression in all forms of senescence using RT-qPCR with primers for amplicons A and F on poly(A)-purified RNA. Late onset activation is shown by comparing days 9 and 20 for OIS and days 12 and 30 for SIPS. (**b**-**e**, **i**-**k**), n = 3 independent biological samples, repeated in 2 independent experiments. Data are mean ±s.d. $*P \leq 0.05$, $**P \leq 0.01$, unpaired two-sided *t*-tests. Exact *P* values can be found in the accompanying Source Data.

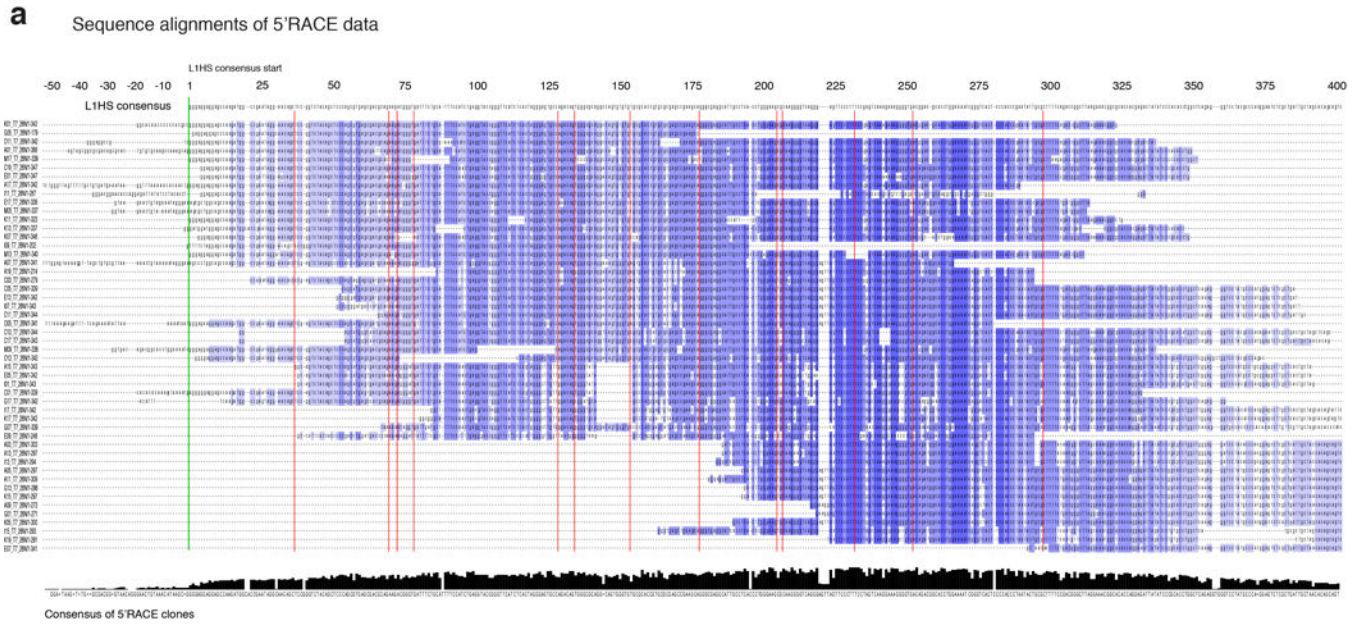


**b** Summary of 5'RACE data

| | | |
|---|---|---|
| Sequenced clones | | 50 |
| Start: < −40 bp | | 4 |
| −25 bp to +25 bp | | 28 |
| +25 bp to +180 bp | | 6 |
| > +180 bp | | 12 |
| **Family** | **Count** | **%** |
| L1HS | 8 | 16 |
| L1PA2 | 9 | 18 |
| L1PA3 | 11 | 22 |
| L1PA4 | 7 | 14 |
| L1PA5 | 8 | 18 |
| L1PA7 | 2 | 4 |
| L1P1 | 5 | 10 |

**Extended Data Figure 2. |. Mapping transcriptional start sites in L1 elements activated during cellular senescence.**

5'RACE was performed with primers C and D (Fig. 1a, Supplementary Table 1) on late senescent cells (16 weeks, point D in Extended Data Fig. 1a), the products were cloned, and individual clones were Sanger sequenced (Methods). **a,** A multiple sequence alignment of the 50 mappable clones against the L1HS consensus was generated with MAFFT software. The L1HS consensus is shown on top. Blue color shading of the aligned clones shows their degree of identity with the consensus. The green vertical line marks the start (position 1) of the L1HS consensus. Red vertical lines mark short gaps (1–4 nucleotides) opened in the L1HS consensus by individual clones. The consensus of the 50 clones is shown at the bottom and was generated with Jalview. The initiation of L1 transcription is known to be imprecise, with the majority of start sites occurring +/−50 bp of the consensus start site, and a subset as far down as +180 bp[68]. **b,** Summary of the mapping data and classification of clones to families of L1 elements. The relative start sites were calculated relative to the L1HS consensus start site. RepEnrich software[55] was used to assign the clones to L1 families.

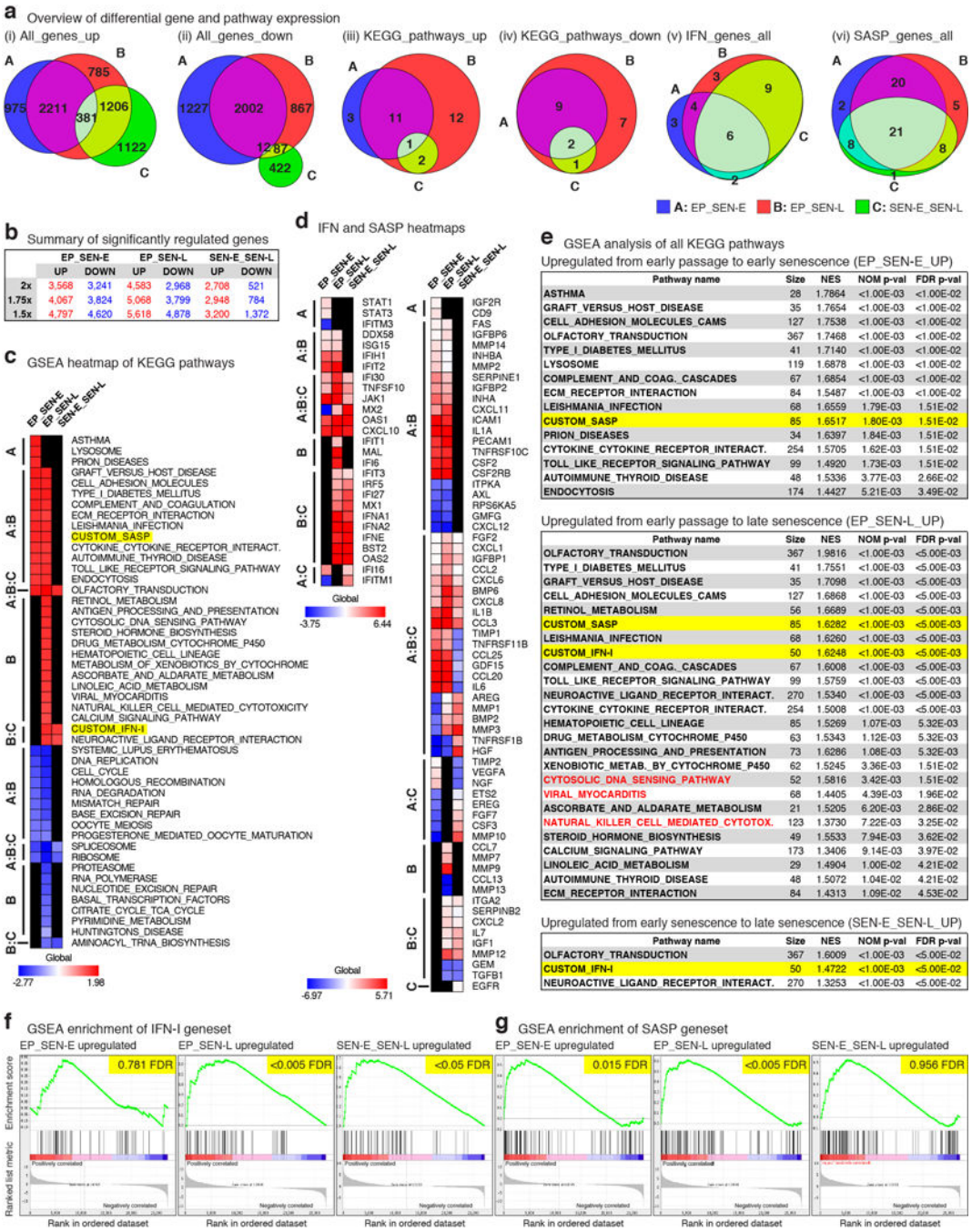


| | EP_SEN-E | | EP_SEN-L | | SEN-E_SEN-L | |
|---|---|---|---|---|---|---|
| | UP | DOWN | UP | DOWN | UP | DOWN |
| 2x | 3,568 | 3,241 | 4,583 | 2,968 | 2,708 | 521 |
| 1.75x | 4,067 | 3,824 | 5,068 | 3,799 | 2,948 | 784 |
| 1.5x | 4,797 | 4,620 | 5,618 | 4,878 | 3,200 | 1,372 |

| Pathway name | Size | NES | NOM p-val | FDR p-val |
|---|---|---|---|---|
| ASTHMA | 28 | 1.7864 | <1.00E-03 | <1.00E-02 |
| GRAFT_VERSUS_HOST_DISEASE | 35 | 1.7654 | <1.00E-03 | <1.00E-02 |
| CELL_ADHESION_MOLECULES_CAMS | 127 | 1.7538 | <1.00E-03 | <1.00E-02 |
| OLFACTORY_TRANSDUCTION | 367 | 1.7468 | <1.00E-03 | <1.00E-02 |
| TYPE_I_DIABETES_MELLITUS | 41 | 1.7140 | <1.00E-03 | <1.00E-02 |
| LYSOSOME | 119 | 1.6878 | <1.00E-03 | <1.00E-02 |
| COMPLEMENT_AND_COAG._CASCADES | 67 | 1.6854 | <1.00E-03 | <1.00E-02 |
| ECM_RECEPTOR_INTERACTION | 84 | 1.5487 | <1.00E-03 | <1.00E-02 |
| LEISHMANIA_INFECTION | 68 | 1.6559 | 1.79E-03 | 1.51E-02 |
| CUSTOM_SASP | 85 | 1.6517 | 1.80E-03 | 1.51E-02 |
| PRION_DISEASES | 34 | 1.6397 | 1.84E-03 | 1.51E-02 |
| CYTOKINE_CYTOKINE_RECEPTOR_INTERACT. | 254 | 1.5705 | 1.62E-03 | 1.51E-02 |
| TOLL_LIKE_RECEPTOR_SIGNALING_PATHWAY | 99 | 1.4920 | 1.73E-03 | 1.51E-02 |
| AUTOIMMUNE_THYROID_DISEASE | 48 | 1.5336 | 3.77E-03 | 2.66E-02 |
| ENDOCYTOSIS | 174 | 1.4427 | 5.21E-03 | 3.49E-02 |

| Pathway name | Size | NES | NOM p-val | FDR p-val |
|---|---|---|---|---|
| OLFACTORY_TRANSDUCTION | 367 | 1.9816 | <1.00E-03 | <5.00E-03 |
| TYPE_I_DIABETES_MELLITUS | 41 | 1.7551 | <1.00E-03 | <5.00E-03 |
| GRAFT_VERSUS_HOST_DISEASE | 35 | 1.7098 | <1.00E-03 | <5.00E-03 |
| CELL_ADHESION_MOLECULES_CAMS | 127 | 1.6868 | <1.00E-03 | <5.00E-03 |
| RETINOL_METABOLISM | 56 | 1.6689 | <1.00E-03 | <5.00E-03 |
| CUSTOM_SASP | 85 | 1.6282 | <1.00E-03 | <5.00E-03 |
| LEISHMANIA_INFECTION | 68 | 1.6260 | <1.00E-03 | <5.00E-03 |
| CUSTOM_IFN-I | 50 | 1.6248 | <1.00E-03 | <5.00E-03 |
| COMPLEMENT_AND_COAG._CASCADES | 67 | 1.6008 | <1.00E-03 | <5.00E-03 |
| TOLL_LIKE_RECEPTOR_SIGNALING_PATHWAY | 99 | 1.5759 | <1.00E-03 | <5.00E-03 |
| NEUROACTIVE_LIGAND_RECEPTOR_INTERACT. | 270 | 1.5340 | <1.00E-03 | <5.00E-03 |
| CYTOKINE_CYTOKINE_RECEPTOR_INTERACT. | 254 | 1.5008 | <1.00E-03 | <5.00E-03 |
| HEMATOPOIETIC_CELL_LINEAGE | 85 | 1.5269 | 1.07E-03 | 5.32E-03 |
| DRUG_METABOLISM_CYTOCHROME_P450 | 63 | 1.5343 | 1.12E-03 | 5.32E-03 |
| ANTIGEN_PROCESSING_AND_PRESENTATION | 73 | 1.6286 | 1.08E-03 | 5.32E-03 |
| XENOBIOTIC_METAB._BY_CYTOCHROME_P450 | 62 | 1.5245 | 3.36E-03 | 1.51E-02 |
| CYTOSOLIC_DNA_SENSING_PATHWAY | 52 | 1.5816 | 3.42E-03 | 1.51E-02 |
| VIRAL_MYOCARDITIS | 68 | 1.4405 | 4.39E-03 | 1.96E-02 |
| ASCORBATE_AND_ALDARATE_METABOLISM | 21 | 1.5205 | 6.20E-03 | 2.86E-02 |
| NATURAL_KILLER_CELL_MEDIATED_CYTOTOX. | 123 | 1.3730 | 7.22E-03 | 3.25E-02 |
| STEROID_HORMONE_BIOSYNTHESIS | 49 | 1.5533 | 7.94E-03 | 3.62E-02 |
| CALCIUM_SIGNALING_PATHWAY | 173 | 1.3406 | 9.14E-03 | 3.97E-02 |
| LINOLEIC_ACID_METABOLISM | 29 | 1.4904 | 1.00E-02 | 4.21E-02 |
| AUTOIMMUNE_THYROID_DISEASE | 48 | 1.5072 | 1.04E-02 | 4.21E-02 |
| ECM_RECEPTOR_INTERACTION | 84 | 1.4313 | 1.09E-02 | 4.53E-02 |

| Pathway name | Size | NES | NOM p-val | FDR p-val |
|---|---|---|---|---|
| OLFACTORY_TRANSDUCTION | 367 | 1.6009 | <1.00E-03 | <5.00E-02 |
| CUSTOM_IFN-I | 50 | 1.4722 | <1.00E-03 | <5.00E-02 |
| NEUROACTIVE_LIGAND_RECEPTOR_INTERACT. | 270 | 1.3253 | <1.00E-03 | <5.00E-02 |

**Extended Data Figure 3. |. Evolution of transcriptomic changes during progression of cellular senescence.**

RNA-seq was performed on early proliferating LF1 cells (EP) and cultures at 8 weeks (SEN-E) and 16 weeks (SEN-L) in senescence (points C and D, respectively, in Extended Data Fig. 1a). Data were analyzed using a 3-way comparison: EP versus SEN-E, EP versus SEN-L and SEN-E versus SEN-L (see Methods for details). **a,** Area-proportional generalized Venn diagrams depicting the intersections of the three comparisons for the following datasets. **i-ii,** significantly upregulated and downregulated genes (row 2x in panel b). **iii-iv,**

significant KEGG pathways identified by GSEA. Note the considerable evolution the transcriptome in late senescence, exemplified by large changes (especially upregulated) in differentially expressed genes as well as pathways. **v-vi,** significantly changing genes in the IFN-I and SASP gene sets (see Supplementary Table 4 for annotation of gene sets). Note that the majority of changes in SASP genes occur early, whereas a large component of IFN-I changes is specific for late senescence. **b,** Summary of significantly changing genes using a fixed FDR (<0.05) and variable fold-change cutoffs (2x, 1.75x and 1.5x). **c,** GSEA analysis of KEGG pathways. Heatmap representation shows significantly upregulated pathways in red (also see panel e) and downregulated pathways in blue. Non-significant comparisons are shown in black; vertical annotations refer to Venn diagrams in (a, iii-iv). Note that the SASP gene set is upregulated early whereas the IFN-I gene set is upregulated late. **d,** Heatmaps of significantly changing genes in the IFN-I and SASP gene sets. Vertical annotations refer to Venn diagrams in (a, v-vi). **e,** List of significantly upregulated KEGG pathways identified using GSEA (see Supplementary Table 5 for a list of all pathways). NES, normalized enrichment scores. IFN-I and SASP genesets are highlighted in yellow. Note the significant upregulation of IFN-I between early and late senescence. Red type identifies KEGG pathways indicative of cytosolic DNA sensing and a type I interferon response at late times. **f-g,** GSEA profiles of the IFN-I and SASP genesets for all comparisons; FDR is highlighted in yellow. Note that the upregulation of IFN-I is significant for EP_SEN-L and SEN-E_SEN-L but not for EP_SEN-E, and that the upregulation of SASP is significant for EP_SEN-E and EP_SEN-L but not SEN-E_SEN-L. n = 3 independent biological samples. Differential expression data were analyzed for significance using the GSEA GenePattern interface and the outputs were corrected for multiple comparisons by adjusting the nominal p values using the Benjamini-Hochberg method (see Methods for details).

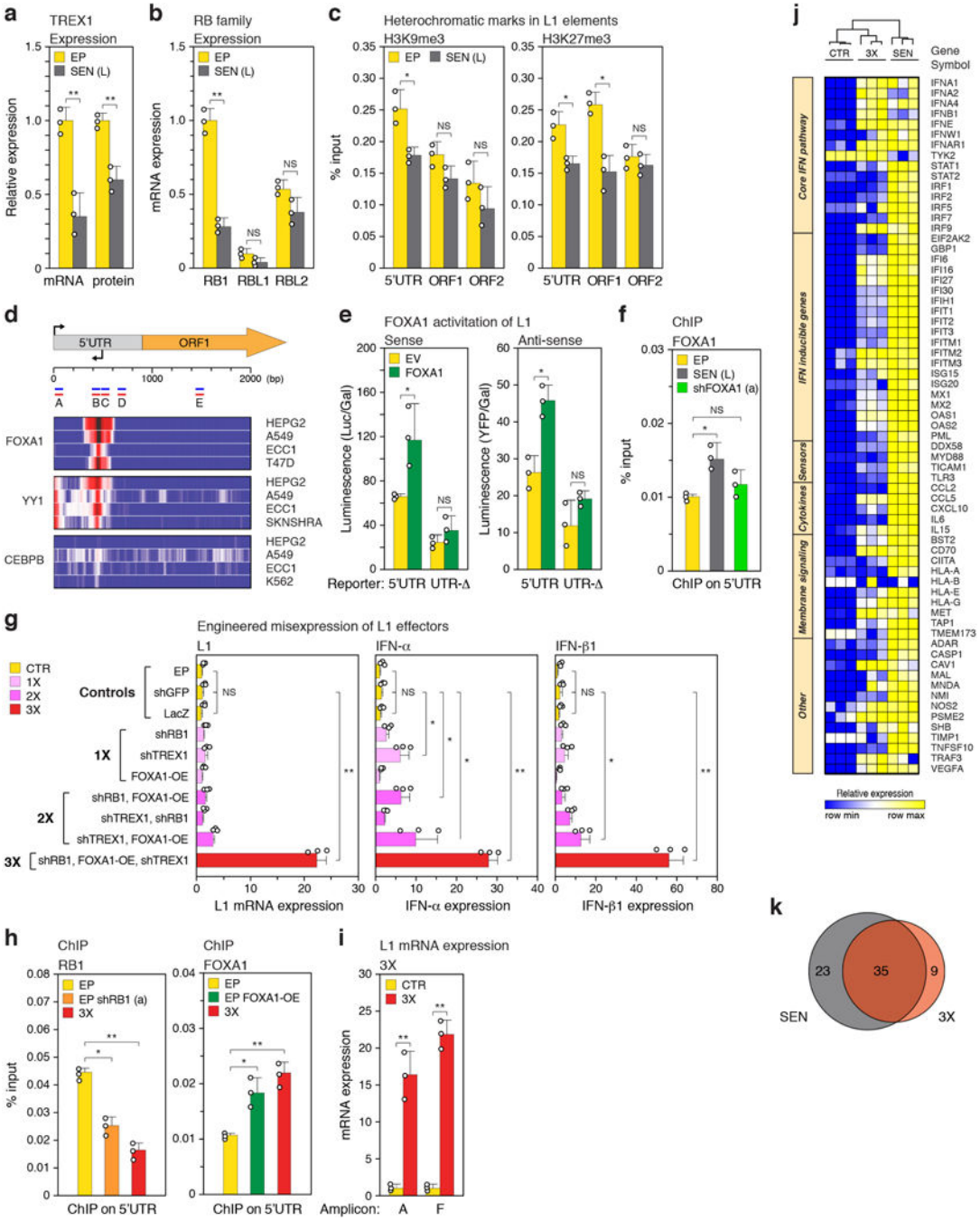


**Extended Data Figure 4. |. Characterization of L1 effectors and the IFN-I response.**

**a,** Expression of TREX1 was determined by RT-qPCR and immunoblotting. For gel source data see Supplementary Fig. 1. **b,** Expression of RB family genes was compared by RT-qPCR. Primer pairs for all genes were verified to be of equivalent efficiency. **c,** Enrichment of H3K9me3 and H3K27me3 on L1 elements was examined by ChIP-qPCR (PCR primers illustrated in Fig. 1b were used: 5'UTR, amplicon A; ORF1, amplicon E; ORF2, amplicon F). **d,** ChIP-seq data from ENCODE were investigated for transcription factors that bind to the L1 consensus sequence. The log2 fold change enrichment relative to input controls is

shown for the indicated cell-lines. The binding of YY1 to the L1 promoter has been documented[69] and was used as a positive control. CEBPB was used as a negative control. A schematic illustrating L1 coordinates and relevant features is shown above. Amplicons A-E are the same as shown in Fig. 1b. **e**, Transcriptional activity of the intact L1 5'UTR or a UTR lacking the FOXA1 binding site (UTR-Δ) was determined using sense and antisense reporters cotransfected into early passage LF1 cells either with a FOXA1 expression plasmid or empty vector (EV). **f,** FOXA1 was knocked down in senescent cells with shFOXA1 (a) (see also Fig. 2e and Extended Data Fig. 5a) and binding to the L1 5'UTR (amplicon B) was determined by ChIP-qPCR. **g,** Knockdown of RB1, TREX1 and ectopic expression of FOXA1 were performed in early passage cells in all single (1X), double (2X) and triple (3X) combinations and assessed by RT-qPCR using poly(A)-purified RNA for activation of L1, IFN-α and IFN-β1 expression (primers for amplicon F). Three controls are shown: cells infected with irrelevant shRNA (shGFP), expression construct (LacZ), or uninfected early passage cells (EP). **h,** L1 5'UTR occupancy of RB1 and FOXA1 in 3X cells was determined by ChIP-qPCR performed as in Fig. 2a, b. Primers for amplicons A and B were used for RB1 and FOXA1, respectively. For comparison, single interventions in early passage cells with shRB1 (a) or FOXA1 cDNA expression (EP FOXA1-OE) are also shown. **i,** Confirmation of full length L1 mRNA expression in 3X cells using RT-qPCR with primers for amplicons A and F on poly(A)-purified RNA. CTR, cells infected with irrelevant shRNA (shGFP). **j**, Heat map representation showing all biological replicates for the 67 genes significantly changing expression in SEN and/or 3X cells (Fig. 2h, Supplementary Table 6). Column clustering was calculated as 1-Pearson correlation. Rows have been grouped into functional subsets of the IFN-I response. **k**, Venn diagram showing the overlap between the 67 significantly changing genes. (**a**-**f**, **h**) n = 3 independent biological samples, repeated in 2 independent experiments. (**g**, **i**), n = 3 independent experiments. (**a**-**i**) Data are mean ±s.d. $*P \leq 0.05$, $**P \leq 0.01$, unpaired two-sided *t*-tests. Exact *P* values can be found in the accompanying Source Data.

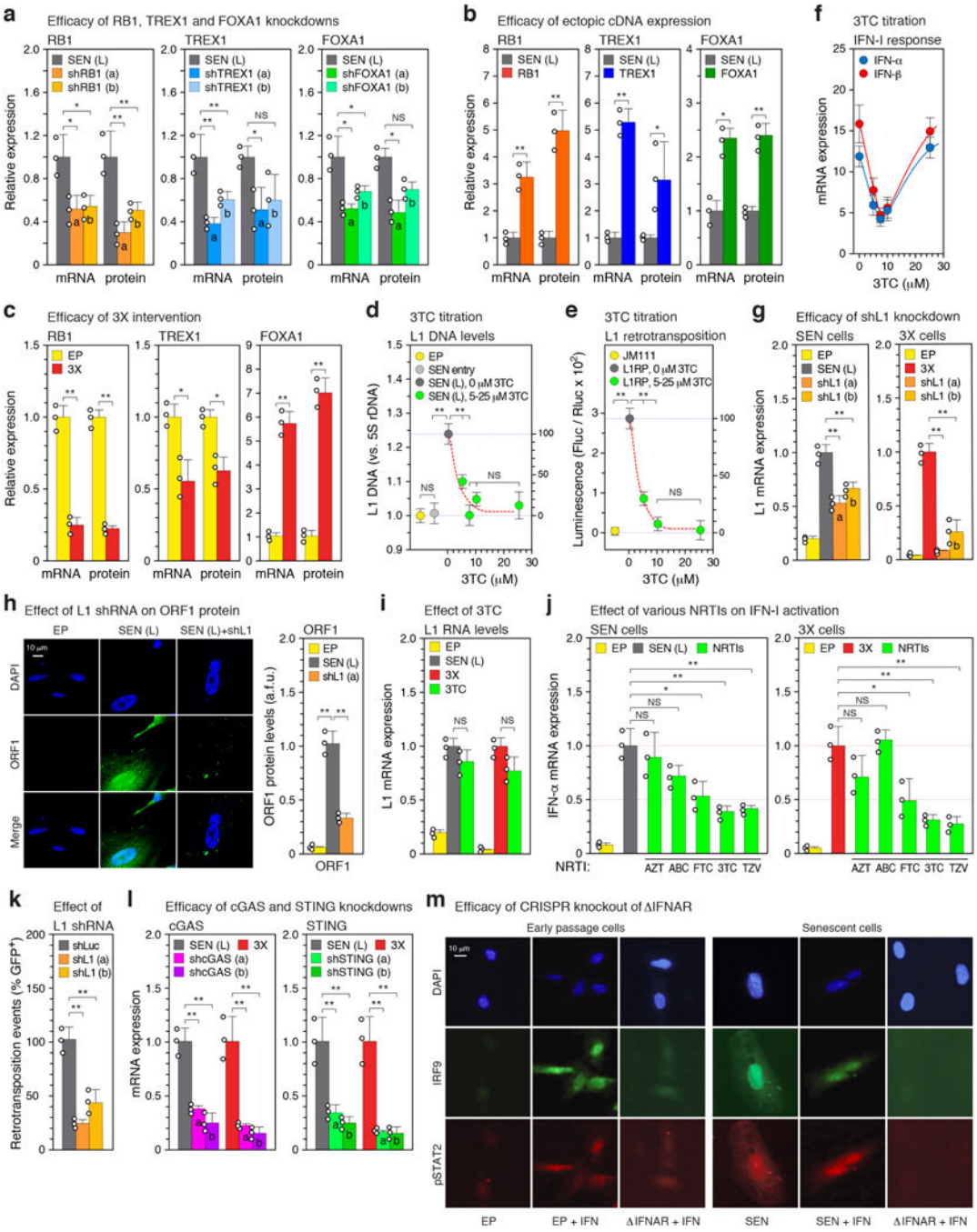


**Extended Data Figure 5. |. Efficacy of genetic and pharmacological interventions.**

**a,** Knockdowns with two distinct shRNAs (a, b) or **b,** ectopic cDNA expression were performed in senescent cells as described in Fig. 2d, e, g (also see Methods). The effectiveness of these manipulations on their targets was assessed by RT-qPCR and immunoblotting. For gel source data see Supplementary Fig. 1. **c,** RB1, TREX1 and FOXA1 mRNA and protein expression after the triple (3X) intervention (Fig. 2f). **d,** The effect of 3TC treatment on the relative abundance of L1HS sequences in senescent cells was determined by multiplex TaqMan qPCR on total DNA (primer set 6, Supplementary Table

1). SEN entry, 0 weeks in senescence (Fig. 1a; point A in Extended Data Fig. 1a). 3TC was administered continuously from SEN entry until harvest 16 weeks later. **e,** The dual luciferase L1 reporter system[52] was used to determine the effect of 3TC dosing on retrotransposition. L1 reporters were introduced into early passage cells using lentivirus vectors (Methods) and cells were treated with 3TC for 4 days prior to harvest and assay. JM111, a defective reporter carrying mutations in ORF1 (absence of 3TC); L1RP, a retrotransposition competent reporter. **f,** The effect of 3TC dosing on the IFN-I response. The experiment above (d) was processed by RT-qPCR to determine the expression of IFN-α and IFN-β1. **g,** Knockdowns of L1 were performed with two distinct shRNAs (a, b) in senescent cells (as in Fig. 2d, e, g) or 3X cells (as in Fig. 2g). The effectiveness on L1 expression was assessed by RT-qPCR using poly(A)-purified RNA and primers F. **h,** Cells in the experiment in (g) were examined for levels of ORF1 protein by immunofluorescence (IF). Image analysis was performed with CellProfiler software (Methods). >200 cells were examined for each condition (a.f.u., arbitrary fluorescence units). **i,** The L1 shRNA treatment in the experiment in (g) was substituted with 3TC treatment (10 μM) for the same period of time. **j,** Five different NRTIs (or combinations) were tested for effects on the IFN-I response. AZT (Zidovudine, 15 μM), ABC (Abacavir, 15 μM), FTC (Emtricitabine, 10 μM), 3TC, (Lamivudine, 10 μM), TZV (Trizivir, a combination of 15 μM AZT, 15 μM ABC and 7.5 μM 3TC). Cells were treated for 4 weeks between 12 and 16 weeks in senescence (Fig. 1a; points D and E in Extended Data Fig. 1a). 3X cells (Fig. 2f) were treated with 3TC for 48 hours after the completion of the last drug selection. Interferon α expression was determined by RT-qPCR. **k,** A native L1 reporter (pLD143)[53] was co-transfected with shRNA plasmid vectors into HeLa cells (Methods). Retrotransposition was scored as GFP-positive cells, and shL1 knockdowns were normalized to a shLuc negative control. The absolute average retrotransposition frequency (percentage of GFP-positive cells) was 4.1, which matches the published values for the reporter used (pLD143)[53]. **l,** Knockdowns of cGAS and STING were performed in senescent or 3X cells as with the other shRNAs (Fig. 2d, e, g and a, g above). **m,** Downregulation of interferon signaling after CRISPR-mediated inactivation of IFNAR1 and IFNAR2 genes was verified by the absence of IRF9 nuclear translocation and STAT2 phosphorylation in response to interferon stimulation. Cells were infected with lentivirus vectors expressing Cas9 and gRNAs to both IFNAR1 and IFNAR2 (ΔIFNAR, Methods). After the infection cells were re-seeded on coverslips, treated with interferon for 2 hours, and examined by IF microscopy. The experiment was repeated 3 times with similar results. (**a**-**i**, **l**) n = 3 independent experiments. (**k**) n = 3 independent biological samples, repeated in 2 independent experiments. (**a**-**l**) Data are mean ±s.d. $*P \leq 0.05$, $**P \leq 0.01$, unpaired two-sided *t*-tests. Exact *P* values can be found in the accompanying Source Data.

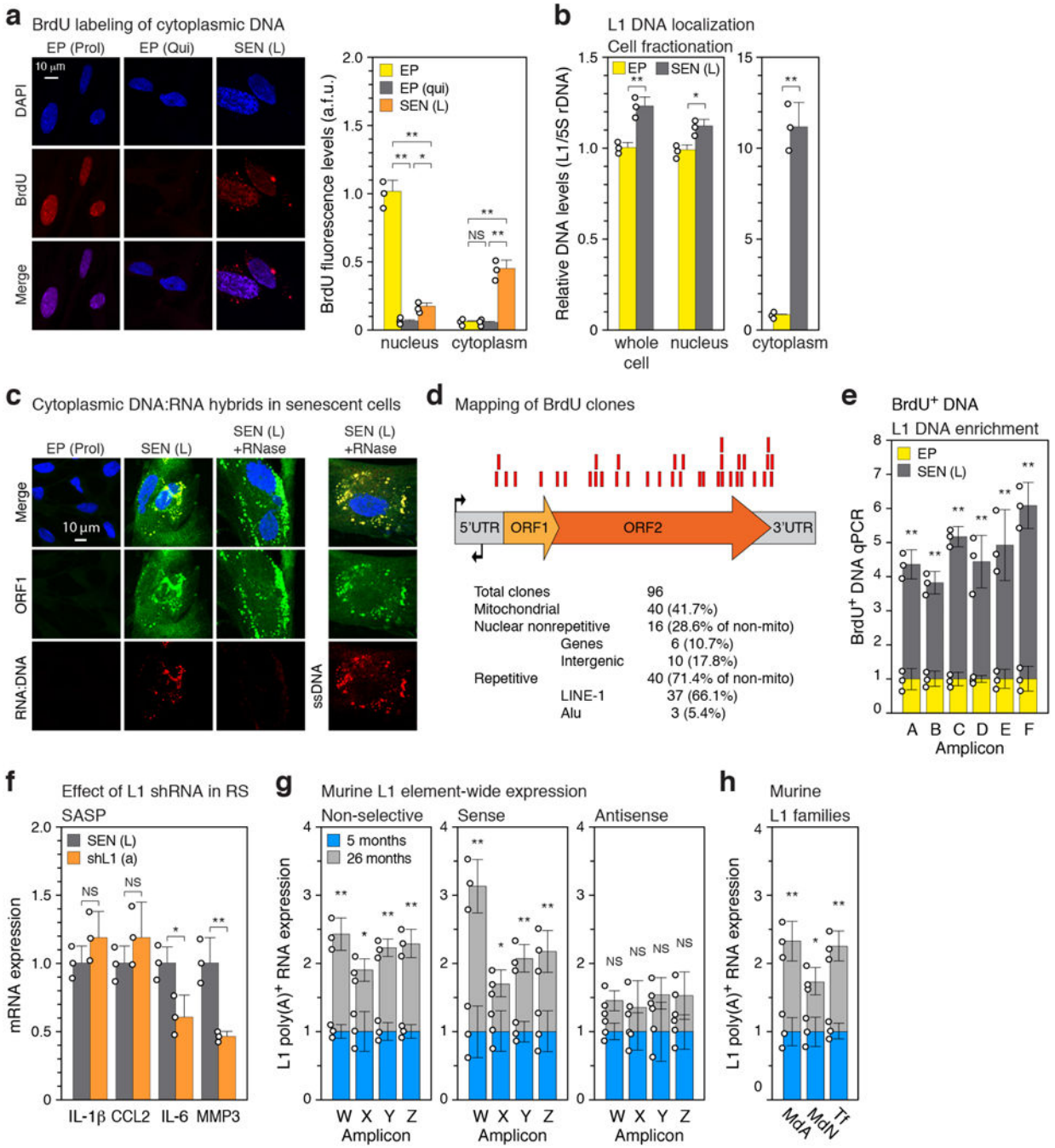


**Extended Data Figure 6. |. Characterization of cytoplasmic DNA in senescent cells.**

**a,** Quiescent and senescent cells were treated with BrdU as in Fig. 3a and the cellular localization of BrdU incorporation was visualized by IF microscopy. Proliferating cells, EP(Prol), are shown as a positive control for nuclear BrdU incorporation. The signals were quantified using CellProfiler software (right panel, Methods). >200 cells were examined for each condition (a.f.u., arbitrary fluorescence units). **b,** Senescent (and EP control) cells (neither labeled with BrdU) were fractionated into nuclear and cytoplasmic fractions, and the representation of L1 sequences in these compartments (as well as whole cells) was

assessed with qPCR as in Fig. 3a (TaqMan multiplex qPCR assay[16], amplicon F, Fig. 1b). Note that the Y axis units differ by 10-fold between the left and right panels. **c,** Cells were examined by IF microscopy for the presence of ORF1 protein, RNA-DNA hybrids, and single-stranded DNA (ssDNA). See Methods and Supplementary Table 2 for antibodies. The RNA-DNA signal in senescent cells largely colocalized with the ORF1 signal and was lost after RNase A treatment. The ssDNA signal also colocalized with the ORF1 signal and was exposed by RNase treatment. The experiment was repeated 3 times with similar results. **d,** The pulled-down BrdU-containing DNA (Fig. 3c, panel (a) above, Methods) was cloned and Sanger sequenced. Of the 96 total clones examined 37 mapped to L1. Red boxes represent the relative positions of these clones on the L1 consensus sequence. **e,** Senescent cells labeled with BrdU (Fig. 3c, panel (a) above) were immunoprecipitated with anti-BrdU antibodies, and the representation of L1 sequences in the pulled-down DNA was assessed using qPCR with primers spanning the entirety of L1 elements (Fig. 1b, c). **f,** Senescent cells were treated with L1 shRNA (using lentiviral vectors as described in Extended Data Fig. 5g) between 12 and 16 weeks of senescence, and expression of SASP genes was determined. **g,** Transcription throughout murine L1 elements was assessed in a strand-specific manner using the same strategy as was applied to human L1 elements (Fig. 1b, c). The amplicons (designated W-Z to distinguish them from the human-specific primers) correspond to the 5'UTR (W), Orf1 (X), Orf2 (Y) and 3'UTR (Z). Also see Methods and Supplementary Table 1 for primer sequences (primer sets 37, 48–50). Poly(A) RNA was prepared from male white adipose tissue. A total of 12 animals were assessed (3 pools of 4 animals each) in 3 independent experiments. **h,** Expression of the three currently active families of murine L1 elements. Primers were designed to distinguishing 5'UTR polymorphisms of the MdA, MdN and Tf families (Methods, Supplementary Table 1 primer sets 51–53). RT-qPCR was performed as in (f) above (non strand-specific). (**a**, **b**, **e**) n = 3 independent biological samples, repeated in 2 independent experiments. (**f**), n = 3 independent experiments. (**a**, **e**-**h**) Data are mean ±s.d. $*P \leq 0.05$, $**P \leq 0.01$. (**a**) 1-way ANOVA with Tukey's multiple comparisons test, (**b**, **e**-**h**) unpaired two-sided *t*-tests, Exact *P* values can be found in the accompanying Source Data.

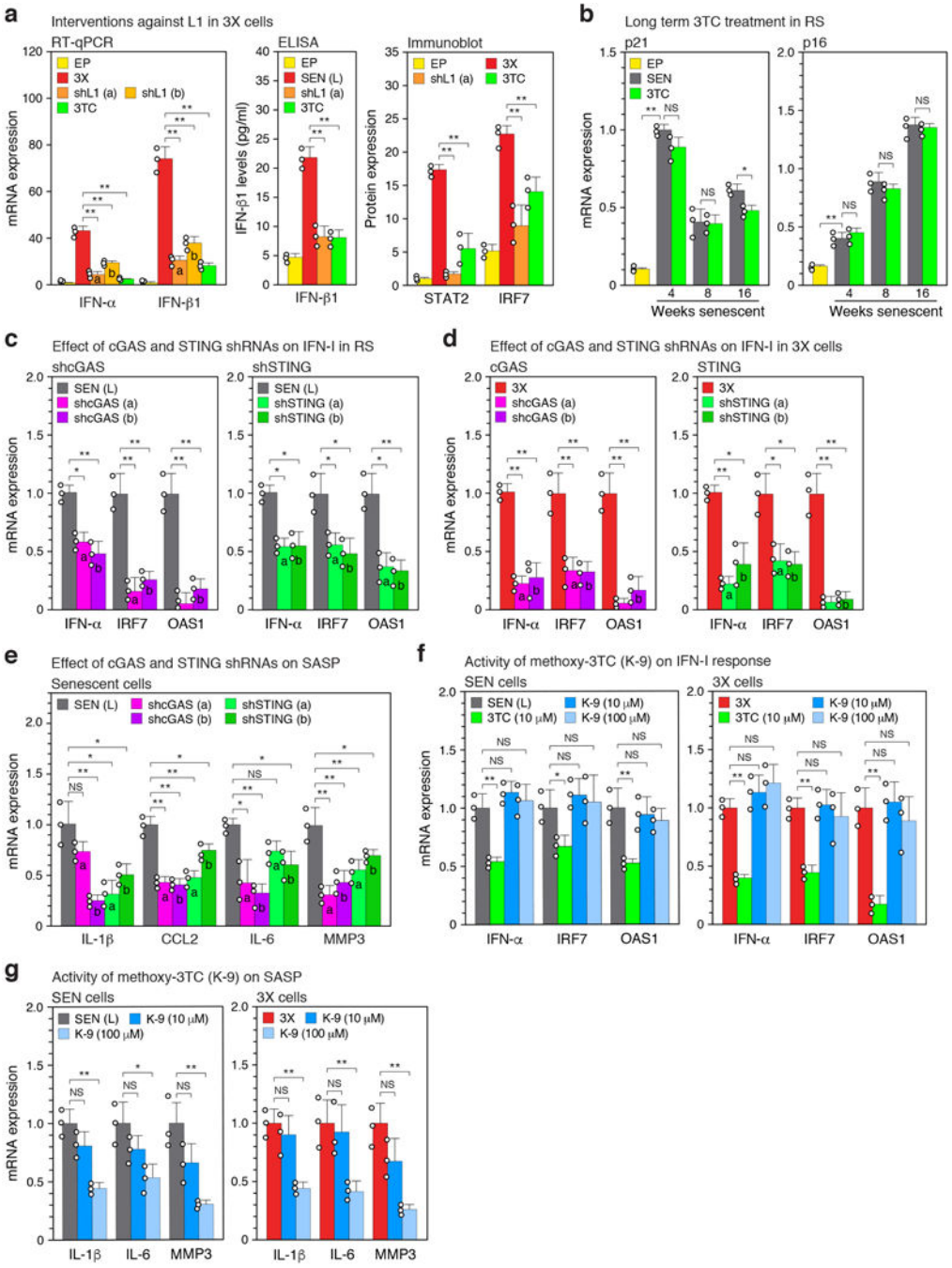


**Extended Data Figure 7. |. Effects of ablating L1 activation, the cytoplasmic DNA sensing pathway, or interferon signaling on expression of the IFN-I and SASP responses.**

**a,** 3X cells were treated with L1 shRNA or with 3TC for 48 hours as described in Extended Data Fig. 5g,i. Effects on the IFN-I response were determined by RT-qPCR, ELISA or immunoblotting. For gel source data see Supplementary Fig. 1. **b,** Cells were serially passaged into replicative senescence (RS) with 3TC (10 μM) present throughout as in Fig. 3f, and expression of Cdk inhibitors p21 and p16 was assessed by RT-qPCR. **c,** Senescent cells were treated with shRNAs against cGAS or STING between 12 and 16 weeks of

senescence (as described in Extended Data Fig. 5l), and expression of IFN-I response genes (IFN-α, IRF7, OAS1) was determined. **d,** cGAS and STING knockdowns were performed with shRNAs in 3X cells (as in panel (c) above), and expression of IFN-I genes was examined by RT-qPCR. **e,** cGAS and STING were knocked down in senescent cells with shRNAs (as in panel (c) above) and expression of SASP response genes (IL-1β, CCL2, IL-6, MMP3) was assayed by RT-qPCR. **f, g,** The activity of K-9 was compared with 3TC in senescent and 3X cells. Senescent cultures were treated between 12 and 16 weeks (as in Fig. 3b) and 3X cultures for 48 hrs. (as in panel (a) above). Effects on the expression of IFN-I genes (IFN-α, IRF7, OAS1) and SASP genes (IL-1β, IL-6, MMP3) was assessed by RT-qPCR. (**a**-**g**), n = 3 independent experiments. (**a**-**g**) Data are mean ±s.d. $*P \leq 0.05$, $**P \leq 0.01$, unpaired two-sided *t*-tests. Exact *P* values can be found in the accompanying Source Data.

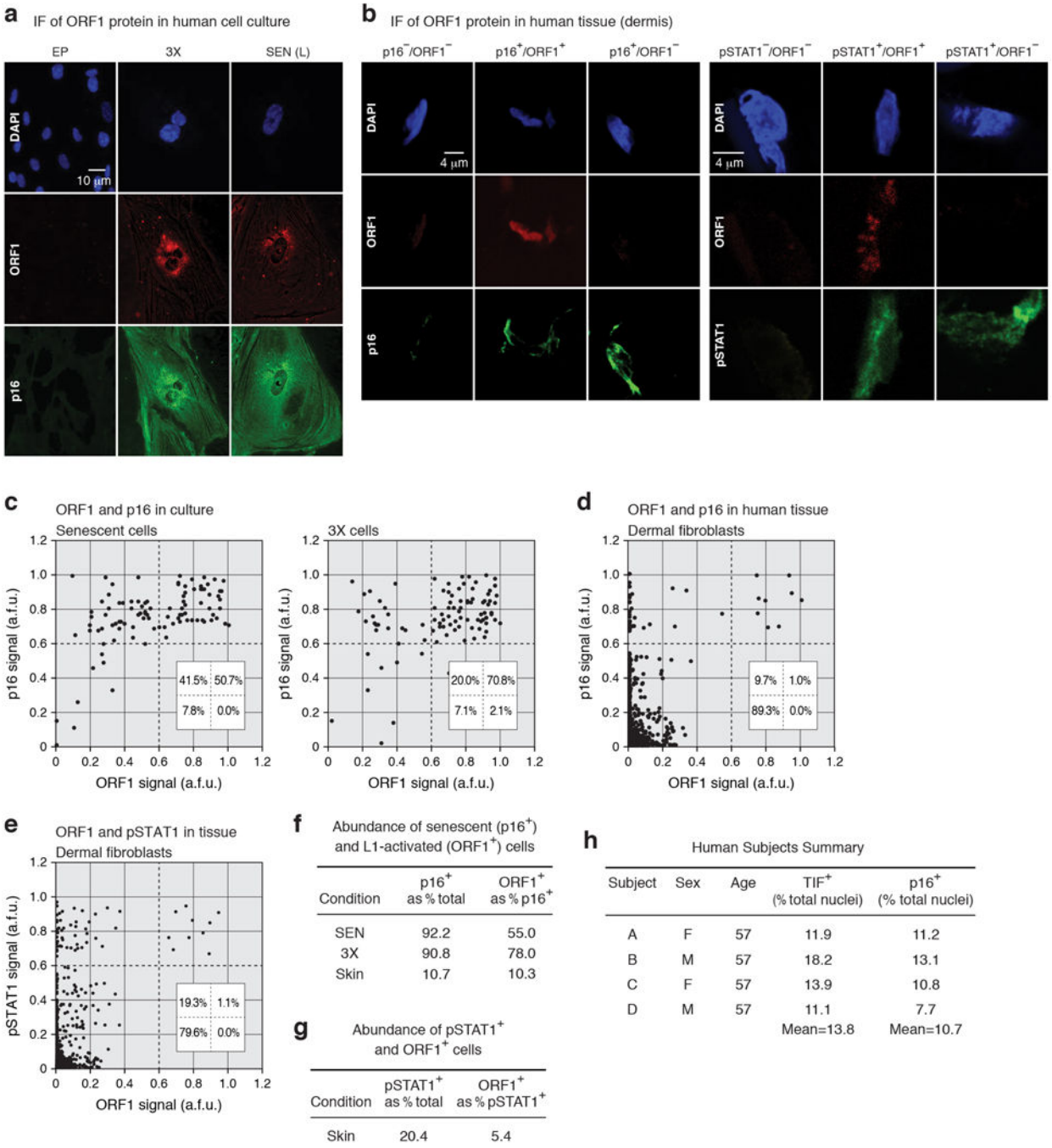


f Abundance of senescent ($p16^+$) and L1-activated ($ORF1^+$) cells

| Condition | $p16^+$ as % total | $ORF1^+$ as % $p16^+$ |
|---|---|---|
| SEN | 92.2 | 55.0 |
| 3X | 90.8 | 78.0 |
| Skin | 10.7 | 10.3 |

g Abundance of $pSTAT1^+$ and $ORF1^+$ cells

| Condition | $pSTAT1^+$ as % total | $ORF1^+$ as % $pSTAT1^+$ |
|---|---|---|
| Skin | 20.4 | 5.4 |

h Human Subjects Summary

| Subject | Sex | Age | $TIF^+$ (% total nuclei) | $p16^+$ (% total nuclei) |
|---|---|---|---|---|
| A | F | 57 | 11.9 | 11.2 |
| B | M | 57 | 18.2 | 13.1 |
| C | F | 57 | 13.9 | 10.8 |
| D | M | 57 | 11.1 | 7.7 |
| | | | Mean=13.8 | Mean=10.7 |

**Extended Data Figure 8. |. Assessment of p16, L1 ORF1 and pSTAT1 expression in senescent cells and skin specimens from aged humans.**

**a**, Immunofluorescence (IF) detection of p16 and ORF1 in early passage, 3X and senescent cells. **b**, Representative images of combinatorial ORF1 and p16 or ORF1p and pSTAT1 staining in human dermis. The experiments shown in panels (a, b) was repeated 3 times independently with similar results. **c**, Cells were plated on cover slips, stained and quantified as described in the Methods. 200 cells in multiple fields were scored for each condition. a.f.u., arbitrary fluorescence units. Insets show the % of cells found in each quadrant. **d, e,**

Abundance of ORF1 and p16 or pSTAT1 cells in human skin. Skin biopsies were cryosectioned and stained as described in the Methods. 200 dermal fibroblast cells in multiple fields were scored for each subject. Aggregated data for 4 subjects (800 cells) are shown. **f**, Data in (c) and (d) were recalculated to show the relative abundance of p16+ cells among all cells, and ORF1+ cells in the p16+ pool of cells. **g,** Data in (e) were recalculated as in (f). **h,** Characteristics of the human subjects used in the analysis of dermal fibroblasts. These specimens were collected as part of the ongoing Leiden Longevity Study[62]. The specimens used here were chosen randomly from left over material. The TIF assay[34] relies on a two-parameter (color) visualization of telomeres (using a FISH probe) and immunofluorescent detection of DNA damage foci (using antibody to 53BP1). Because of limiting material it was not possible to combine detection of p16 with TIFs in a 3 color experiment.

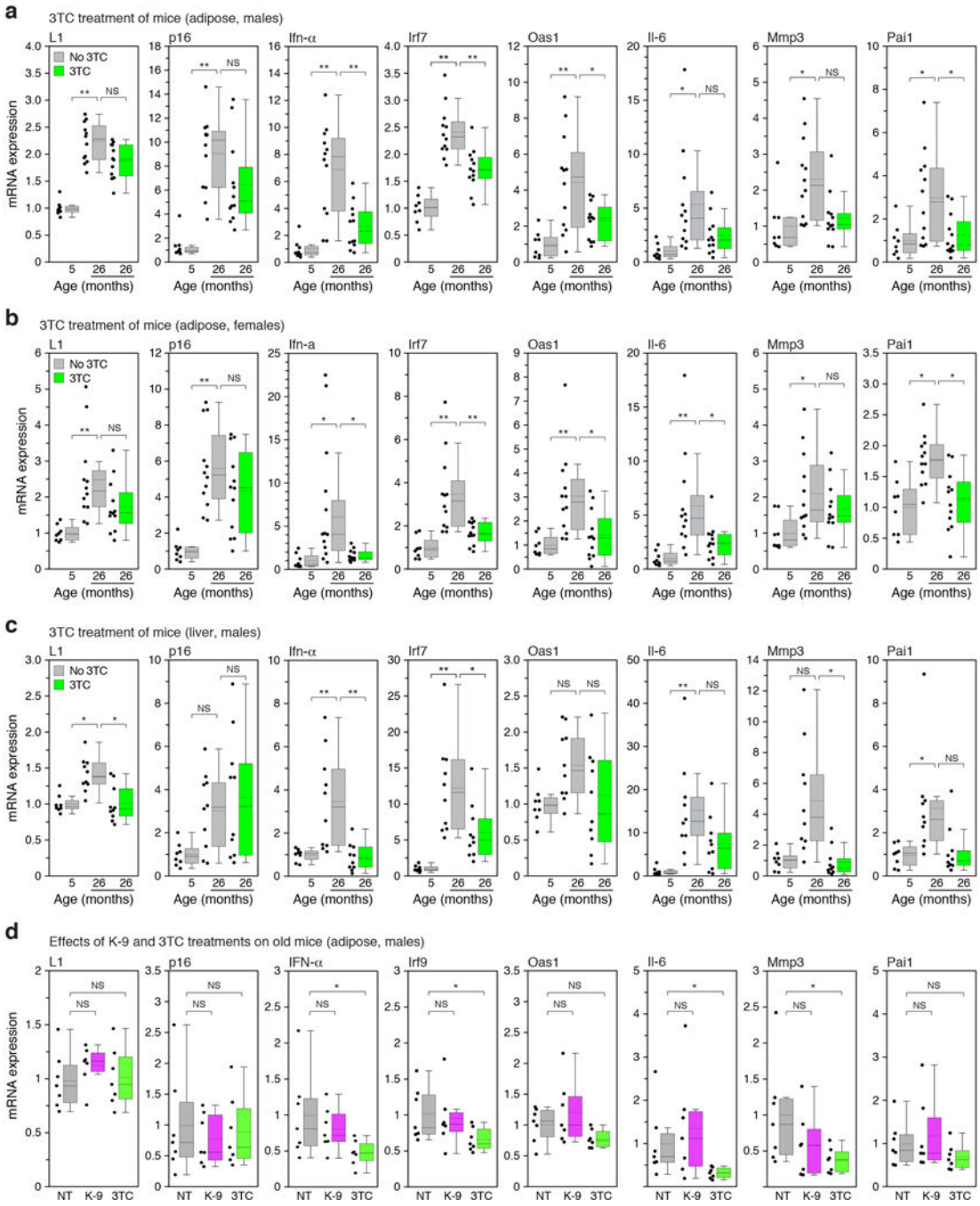


**Extended Data Figure 9. |. Effects of 3TC or K-9 treatment on L1, p16, IFN-I and SASP gene expression in mouse tissues.**

**a-c,** Mice at the indicated ages were treated with 3TC continuously for two weeks (see also Fig. 4c, e, Extended Data Fig. 10d-f, and Methods). For all conditions the expression of L1 mRNA, p16, three representative IFN-I response genes (Ifn-α, Irf7, Oas1) and three representative SASP genes (Il-6, Mmp3, Pai1) were assessed by RT-qPCR. In no instance was expression at 5 months + 3TC significantly different from the no drug control, therefore these data are not shown in the figure (for all collected data see Supplementary Table 7). The box plots show the range of the data (whiskers), 25th and 75 percentiles (box), means

(dashed line), and medians (solid line). Each point represents one animal. **a,** Visceral white adipose, male mice. 5 months, n=8 animals; 26 months, n=12 animals; 26 months + 3TC, n=12 animals. **b,** Visceral white adipose, female mice. 5 months, n=8 animals; 26 months, n=12 animals; 26 months + 3TC, n=12 animals. **c,** Liver, male mice. 5 months, n=8 animals; 26 months, n=10 animals; 26 months + 3TC, n=10 animals. **d,** Mice at the age of 26 months were treated with K-9 or 3TC in drinking water for two weeks and analyzed by RT-qPCR as above. NT, not treated. Visceral white adipose, male mice, n=7 animals for each group. Data are mean ±s.d. *$P \leq 0.05$, **$P \leq 0.01$, 1-way ANOVA with Tukey's multiple comparisons test. Exact $P$ values can be found in the accompanying Source Data.

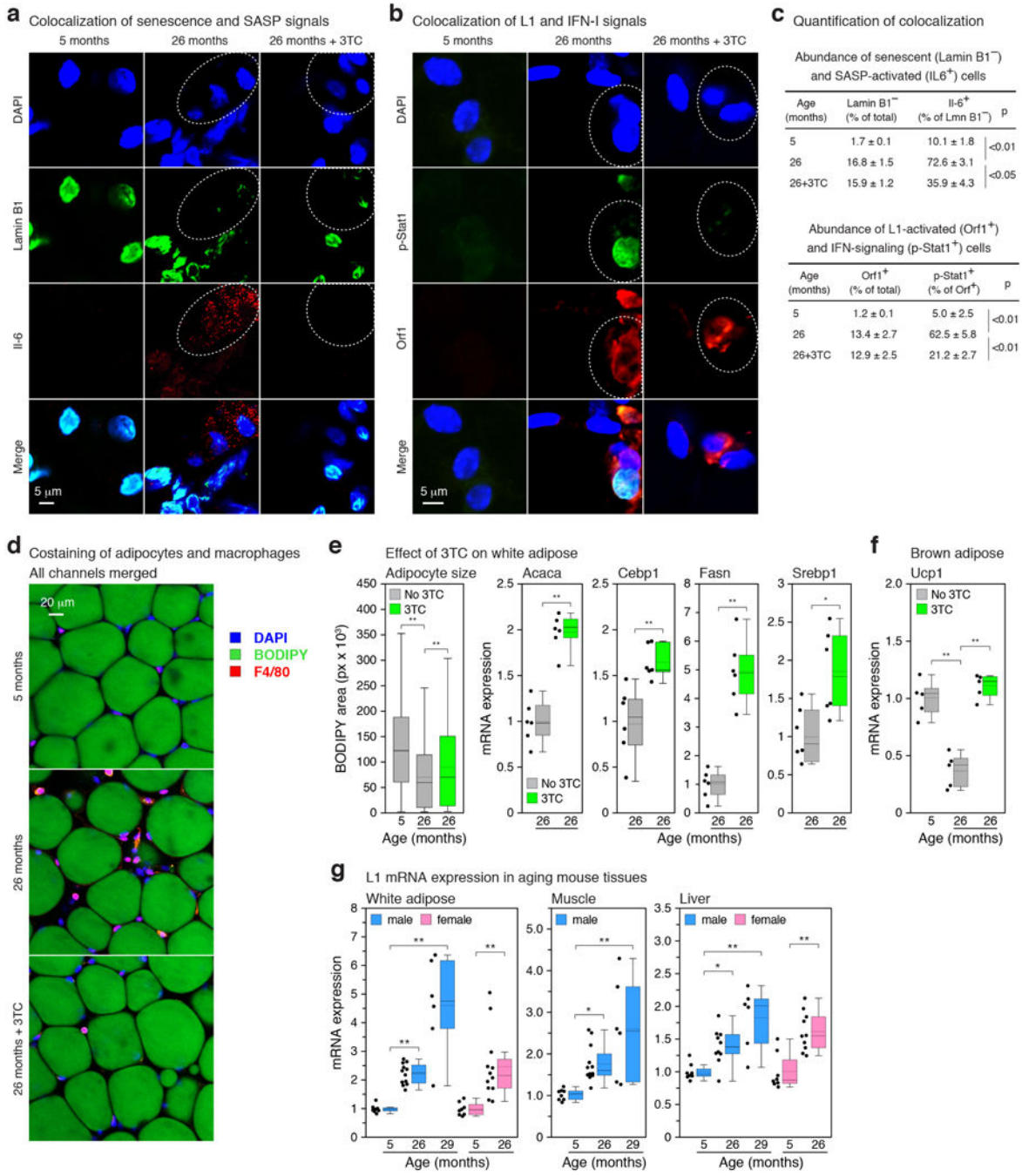


**Extended Data Figure 10. |. Combinatorial assessment of senescence, IFN-I, SASP and L1 markers and effects of 3TC on age-associated phenotypes in mouse tissues.**

**a, b,** Whole-mount IF was performed on white adipose of 5 months and 26 months old (with and without 2 weeks of 3TC treatment) male mice. In (a) loss of Lamin B1 (senescence marker) was colocalized with IL-6 (SASP marker). In (b) pStat1 (IFN-I marker) was colocalized with Orf1 (L1 marker). **c,** Quantification of the experiments shown in (a) and (b). 4 animals and at least 200 cells per animal were scored for each condition. **d**, Neutral lipids were stained with BODIPY to visualize mature adipocytes in whole-mount

preparations, and macrophages were detected by IF using the F4/80 antibody. **e,** The effects of 2 weeks of 3TC treatment on adipogenesis were assessed by measuring mean adipocyte size (left panel), and by RT-qPCR to determine the expression of key adipogenic genes (right panels; Acaca, acetyl-CoA carboxylase 1; Cebp1, CCAAT/enhancer-binding protein alpha; Fasn, fatty acid synthase; Srebp1, sterol regulatory element-binding protein 1). The box plots show the range of the data (whiskers), 25th and 75 percentiles (box), means (dashed line), and medians (solid line). Adipocyte size (BODIPY-stained area) was calculated using CellProfiler; aggregated data for 5 animals and 500 total cells are shown. For RT-qPCR data each point represents one animal; n = 6 animals. **f,** Expression of the Ucp1 gene (thermogenin) in brown adipose tissue was determined by RT-qPCR and is represented as in (e). n = 5 animals. **g,** Expression of L1 mRNA was determined by RT-qPCR and is represented as in (e). 5 months, n=8 animals; 26 months, n=12 animals; 29 months, n=6 animals. (**e**-**g**) Data are mean ±s.d. $*P \leq 0.05$, $**P \leq 0.01$. (**c**, **e** left panel, **f**, **g**) 1-way ANOVA with Tukey's multiple comparisons test, (**e** right panels) unpaired two-sided *t*-tests. Exact *P* values can be found in the accompanying Source Data.

## Supplementary Material

Refer to Web version on PubMed Central for supplementary material.

## Acknowledgments.

The following funding sources are acknowledged: M.D., Glenn/AFAR Postdoctoral Fellowship, NIH P20 GM119943 COBRE pilot award; T.I., NIH F31 AG043189; A.P.P. and A.E.E., NIH T32 AG041688; S.W.C., NIH F31 AG050365; A.C. and G.B., Biotechnology and Sport Medicine Fellowships, School of Pharmacy, University of Bologna, Bologna, Italy; E.M.A, and J.D.B., NIH P01 AG051449; C.B., Canadian Institute of Health Research MOP-102709; J.A., NIH DP1 GM114862, R01 EY022238, R01 EY024068, R01 EY028027, John Templeton Foundation Grant ID 60763; M.S., A.S. and V.G., NIH R01 AG046320, R01 AG027237, R01 AG047200, P01 AG051449, Life Extension Foundation; S.L.H., NIH R37 AG016667, R01 AG024353, P01 AG051449, Glenn-AFAR Breakthroughs in Gerontology Award; N.N., NIH R01 AG050582, P20 GM109035; J.M.S., NIH R37 AG016694, P01 AG051449. We are grateful to Andrea Maier, Mariette Waaijer, Rudi Westendorp and the participants of the Leiden Longevity Study (LLS) for assistance with the human specimens. The biomaterials collection of the LLS (P. Eline Slagboom, principal investigator) was supported by the Netherlands Genomics Initiative of the Netherlands Organization for Scientific Research (NWO), within the framework of the Netherlands Consortium of Healthy Ageing (NCHA, 050–060-810) and the Leiden University Medical Center.

## References

1. Huang CR, Burns KH & Boeke JD Active transposition in genomes. Annu. Rev. Genet. 46, 651–75 (2012). [PubMed: 23145912]
2. de Koning AP et al. Repetitive elements may comprise over two-thirds of the human genome. PLoS Genet. 7, e1002384 (2011). [PubMed: 22144907]
3. Hancks DC & Kazazian HH Jr Active human retrotransposons: variation and disease. Curr. Opin. Genet. Dev. 22, 191–203 (2012). [PubMed: 22406018]
4. Rodic N et al. Long interspersed element-1 protein expression is a hallmark of many human cancers. Am. J. Pathol. 184, 1280–6 (2014). [PubMed: 24607009]
5. Erwin JA, Marchetto MC & Gage FH Mobile DNA elements in the generation of diversity and complexity in the brain. Nat. Rev. Neurosci. 15, 497–506 (2014). [PubMed: 25005482]
6. De Cecco M et al. Genomes of replicatively senescent cells undergo global epigenetic changes leading to gene silencing and activation of transposable elements. Aging Cell 12, 247–256 (2013). [PubMed: 23360310]
7. Van Meter M et al. SIRT6 represses LINE1 retrotransposons by ribosylating KAP1 but this repression fails with stress and age. Nat Commun 5, 5011 (2014). [PubMed: 25247314]

8. Kreiling JA et al. Contribution of retrotransposable elements to aging in Human Retrotransposons in Health and Disease (ed. Cristofari G) 297–321 (Springer International, 2017).
9. Volkman HE & Stetson DB The enemy within: endogenous retroelements and autoimmune disease. Nat. Immunol. 15, 415–22 (2014). [PubMed: 24747712]
10. Salama R, Sadaie M, Hoare M & Narita M Cellular senescence and its effector programs. Genes Dev 28, 99–114 (2014). [PubMed: 24449267]
11. Thomas CA et al. Modeling of TREX1-dependent autoimmune disease using human stem cells highlights L1 accumulation as a source of neuroinflammation. Cell Stem Cell 21, 319–331 e8 (2017). [PubMed: 28803918]
12. Ishak CA et al. An RB-EZH2 complex mediates silencing of repetitive DNA sequences. Mol Cell 64, 1074–1087 (2016). [PubMed: 27889452]
13. Li Q et al. FOXA1 mediates p16(INK4a) activation during cellular senescence. EMBO J. 32, 858–73 (2013). [PubMed: 23443045]
14. Denli AM et al. Primate-specific ORF0 contributes to retrotransposon-mediated diversity. Cell 163, 583–93 (2015). [PubMed: 26496605]
15. Dai L, Huang Q & Boeke JD Effect of reverse transcriptase inhibitors on LINE-1 and Ty1 reverse transcriptase activities and on LINE-1 retrotransposition. BMC Biochem. 12, 18 (2011). [PubMed: 21545744]
16. Coufal NG et al. L1 retrotransposition in human neural progenitor cells. Nature 460, 1127–31 (2009). [PubMed: 19657334]
17. Dhanwani R, Takahashi M & Sharma S Cytosolic sensing of immuno-stimulatory DNA, the enemy within. Curr Opin Immunol 50, 82–87 (2017). [PubMed: 29247853]
18. Fowler BJ et al. Nucleoside reverse transcriptase inhibitors possess intrinsic anti-inflammatory activity. Science 346, 1000–3 (2014). [PubMed: 25414314]
19. Herbig U et al. Cellular senescence in aging primates. Science 311, 1257 (2006). [PubMed: 16456035]
20. Coppe JP, Desprez PY, Krtolica A & Campisi J The senescence-associated secretory phenotype: the dark side of tumor suppression. Annu. Rev. Pathol. 5, 99–118 (2010). [PubMed: 20078217]
21. Chang J et al. Clearance of senescent cells by ABT263 rejuvenates aged hematopoietic stem cells in mice. Nat Med 22, 78–83 (2016). [PubMed: 26657143]
22. Zhu Y et al. The Achilles' heel of senescent cells: from transcriptome to senolytic drugs. Aging Cell 14, 644–58 (2015). [PubMed: 25754370]
23. Tchkonia T et al. Fat tissue, aging, and cellular senescence. Aging Cell 9, 667–84 (2010). [PubMed: 20701600]
24. Mattson MP Perspective: Does brown fat protect against diseases of aging? Ageing Res Rev 9, 69–76 (2010). [PubMed: 19969105]
25. Frasca D & Blomberg BB Inflammaging decreases adaptive and innate immune responses in mice and humans. Biogerontology 17, 7–19 (2016). [PubMed: 25921609]
26. Baker DJ et al. Naturally occurring p16(Ink4a)-positive cells shorten healthy lifespan. Nature 530, 184–9 (2016). [PubMed: 26840489]
27. Baker DJ et al. Clearance of p16Ink4a-positive senescent cells delays ageing-associated disorders. Nature 479, 232–6 (2011). [PubMed: 22048312]
28. West AP & Shadel GS Mitochondrial DNA in innate immune responses and inflammatory pathology. Nat Rev Immunol 17, 363–375 (2017). [PubMed: 28393922]
29. Dou Z et al. Cytoplasmic chromatin triggers inflammation in senescence and cancer. Nature 550, 402–406 (2017). [PubMed: 28976970]
30. Takahashi A et al. Downregulation of cytoplasmic DNases is implicated in cytoplasmic DNA accumulation and SASP in senescent cells. Nat Commun 9, 1249 (2018). [PubMed: 29593264]
31. Franceschi C & Campisi J Chronic inflammation (inflammaging) and its potential contribution to age-associated diseases. J. Gerontol. A Biol. Sci. Med. Sci. 69 Suppl 1, S4–9 (2014). [PubMed: 24833586]
32. Lopez-Otin C et al. The hallmarks of aging. Cell 153, 1194–217 (2013). [PubMed: 23746838]

33. Brown JP, Wei W & Sedivy JM Bypass of senescence after disruption of p21CIP1/WAF1 gene in normal diploid human fibroblasts. Science 277, 831–4 (1997). [PubMed: 9242615]
34. Herbig U et al. Telomere shortening triggers senescence of human cells through a pathway involving ATM, p53, and p21(CIP1), but not p16(INK4a). Mol. Cell 14, 501–13 (2004). [PubMed: 15149599]
35. Fumagalli M, Rossiello F, Mondello C & d'Adda di Fagagna F Stable cellular senescence is associated with persistent DDR activation. PLoS One 9, e110969 (2014). [PubMed: 25340529]
36. Ambati J, Fowler B & Ambati K Compositions and Methods for Treating Retinal Degradation. in PCT Patent Publication WO/2016/138425 (2016).
37. Else LJ et al. Pharmacokinetics of lamivudine and lamivudine-triphosphate after administration of 300 milligrams and 150 milligrams once daily to healthy volunteers: results of the ENCORE 2 study. Antimicrob. Agents Chemother. 56, 1427–33 (2012). [PubMed: 22183172]
38. Le ON et al. Ionizing radiation-induced long-term expression of senescence markers in mice is independent of p53 and immune status. Aging Cell 9, 398–409 (2010). [PubMed: 20331441]
39. Li W et al. The EMBL-EBI bioinformatics web and programmatic tools framework. Nucleic Acids Res. 43, W580–4 (2015). [PubMed: 25845596]
40. Ye J et al. Primer-BLAST: a tool to design target-specific primers for polymerase chain reaction. BMC Bioinf. 13, 134 (2012).
41. Gautier G et al. A type I interferon autocrine-paracrine loop is involved in Toll-like receptor-induced interleukin-12p70 secretion by dendritic cells. J. Exp. Med. 201, 1435–46 (2005). [PubMed: 15851485]
42. Kim D, Langmead B & Salzberg SL HISAT: a fast spliced aligner with low memory requirements. Nat Methods 12, 357–60 (2015). [PubMed: 25751142]
43. Liao Y, Smyth GK & Shi W featureCounts: an efficient general purpose program for assigning sequence reads to genomic features. Bioinformatics 30, 923–30 (2014). [PubMed: 24227677]
44. Robinson MD, McCarthy DJ & Smyth GK edgeR: a Bioconductor package for differential expression analysis of digital gene expression data. Bioinformatics 26, 139–140 (2010). [PubMed: 19910308]
45. Reich M et al. GenePattern 2.0. Nat Genet 38, 500–1 (2006). [PubMed: 16642009]
46. Subramanian A et al. Gene set enrichment analysis: a knowledge-based approach for interpreting genome-wide expression profiles. Proc Natl Acad Sci U S A 102, 15545–50 (2005). [PubMed: 16199517]
47. Benjamini Y & Hochberg Y Controlling the false discovery rate: a practical and powerful approach to multiple testing. J Roy Stat Soc B 57, 289–300 (1995).
48. Langmead B Aligning short sequencing reads with Bowtie. Curr. Protoc. Bioinformatics Chapter 11, Unit 11.7 (2010).
49. Alexandrova EA et al. Sense transcripts originated from an internal part of the human retrotransposon LINE-1 5' UTR. Gene 511, 46–53 (2012). [PubMed: 22982412]
50. Olovnikov IA et al. A key role of the internal region of the 5'-untranslated region in the human L1 retrotransposon transcription activity. Mol. Biol. (Mosk) 41, 508–14 (2007).
51. Michaud K et al. Pharmacologic inhibition of cyclin-dependent kinases 4 and 6 arrests the growth of glioblastoma multiforme intracranial xenografts. Cancer Res. 70, 3228–38 (2010). [PubMed: 20354191]
52. Xie Y et al. Characterization of L1 retrotransposition with high-throughput dual-luciferase assays. Nucleic Acids Res 39, e16 (2011). [PubMed: 21071410]
53. An W et al. Characterization of a synthetic human LINE-1 retrotransposon ORFeus-Hs. Mob DNA 2, 2 (2011). [PubMed: 21320307]
54. Penzkofer T, Dandekar T & Zemojtel T L1Base: from functional annotation to prediction of active LINE-1 elements. Nucleic Acids Res 33, D498–500 (2005). [PubMed: 15608246]
55. Criscione SW et al. Transcriptional landscape of repetitive elements in normal and cancer human cells. BMC Genomics 15, 583 (2014). [PubMed: 25012247]
56. Childs BG, Durik M, Baker DJ & van Deursen JM Cellular senescence in aging and age-related disease: from mechanisms to therapy. Nat. Med. 21, 1424–35 (2015). [PubMed: 26646499]

57. Katoh K & Standley DM MAFFT multiple sequence alignment software version 7: improvements in performance and usability. Mol Biol Evol 30, 772–80 (2013). [PubMed: 23329690]
58. Waterhouse AM et al. Jalview Version 2--a multiple sequence alignment editor and analysis workbench. Bioinformatics 25, 1189–91 (2009). [PubMed: 19151095]
59. Sanjana NE, Shalem O & Zhang F Improved vectors and genome-wide libraries for CRISPR screening. Nat. Methods 11, 783–4 (2014). [PubMed: 25075903]
60. Shalem O et al. Genome-scale CRISPR-Cas9 knockout screening in human cells. Science 343, 84–7 (2014). [PubMed: 24336571]
61. Kreiling JA et al. Age-associated increase in heterochromatic marks in murine and primate tissues. Aging Cell 10, 292–304 (2011). [PubMed: 21176091]
62. Schoenmaker M et al. Evidence of genetic enrichment for exceptional survival using a family approach: the Leiden Longevity Study. Eur. J. Hum. Genet. 14, 79–84 (2006). [PubMed: 16251894]
63. Waaijer ME et al. The number of p16INK4a positive cells in human skin reflects biological age. Aging Cell 11, 722–5 (2012). [PubMed: 22612594]
64. Kamentsky L et al. Improved structure, function and compatibility for CellProfiler: modular high-throughput image analysis software. Bioinformatics 27, 1179–80 (2011). [PubMed: 21349861]
65. Martinez-Santibanez G, Cho KW & Lumeng CN Imaging white adipose tissue with confocal microscopy. Methods Enzymol 537, 17–30 (2014). [PubMed: 24480339]
66. Itahana K, Campisi J & Dimri GP Methods to detect biomarkers of cellular senescence: the senescence-associated beta-galactosidase assay. Methods Mol. Biol. 371, 21–31 (2007). [PubMed: 17634571]
67. Schorl C & Sedivy JM Analysis of cell cycle phases and progression in cultured mammalian cells. Methods 41, 143–50 (2007). [PubMed: 17189856]
68. Rangwala SH, Zhang L & Kazazian HH Jr. Many LINE1 elements contribute to the transcriptome of human somatic cells. Genome Biol 10, R100 (2009). [PubMed: 19772661]
69. Athanikar JN, Badge RM & Moran JV A YY1-binding site is required for accurate human LINE-1 transcription initiation. Nucleic Acids Res. 32, 3846–55 (2004). [PubMed: 15272086]

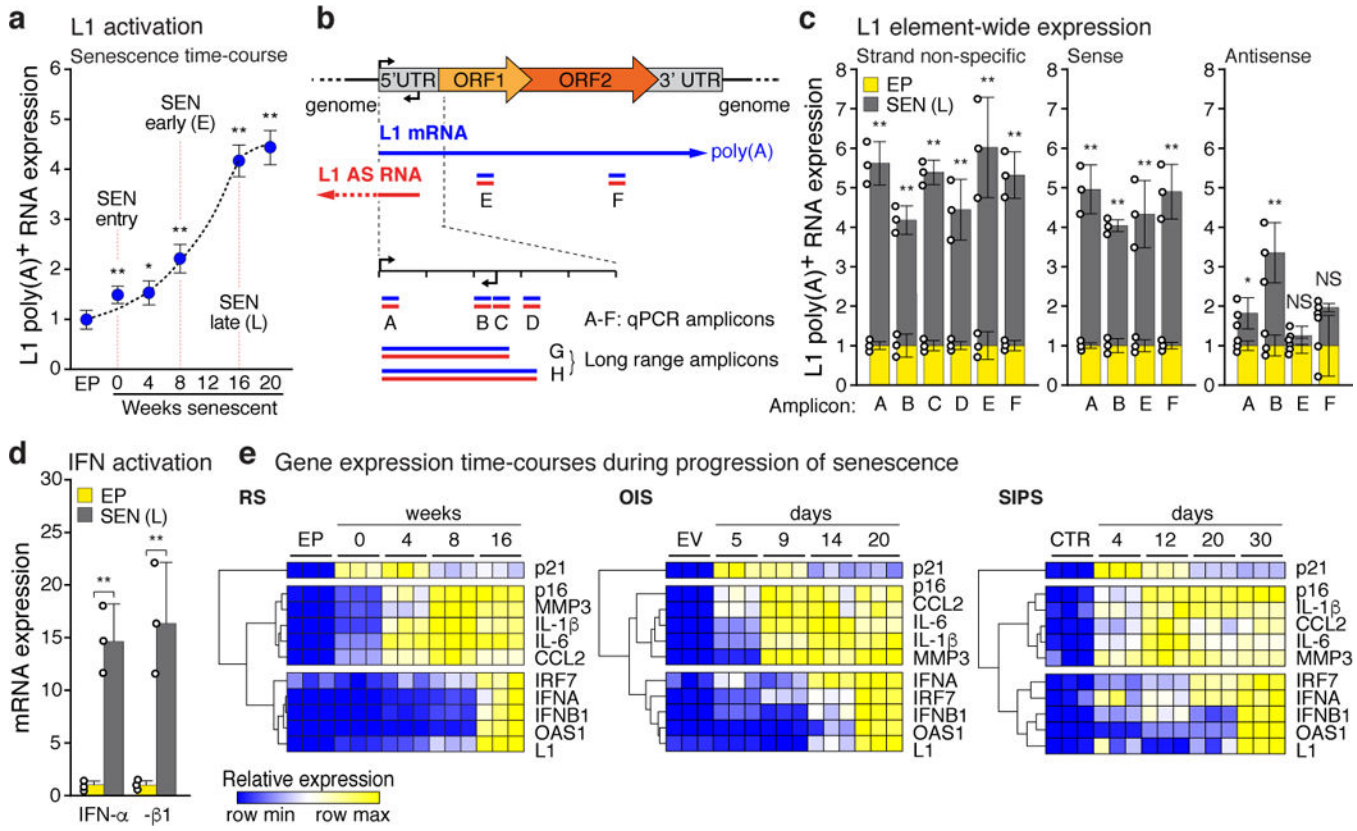


**Figure 1 |. Activation of L1, IFN-I and SASP in senescent cells.**

Gene expression was assessed by RT-qPCR. Poly(A)-purified RNA was used in all L1 assays. **a,** Time course of L1 activation. *P* values were calculated relative to EP, early passage control. **b**, Schematic of L1 RT-PCR strategy. Blue, sense; red, antisense (AS). For primer specificity see Extended Data Fig. 1f-h; primer design see Methods. Primers for amplicon F were used in (**a**) and (**e**). **c**, Strand-specific L1 transcription was assessed using amplicons A-F. Transcription from the 5'UTR antisense promoter was also detected. SEN (L), late senescence (16 weeks). **d**, Induction of IFN-α and IFN-β1 mRNA levels. **e**, The temporal induction of genes associated with DNA damage (p21), SASP (IL-1β, CCL2, IL-6, MMP3), and the IFN-I response (IRF7, IFN-α, IFN-β1, OAS1). Row clustering was calculated as 1-Pearson correlation. RS, replicative senescence; OIS, oncogene induced senescence (elicited by Ha-RAS infection); SIPS, stress induced premature senescence (gamma irradiation). Controls: EP, early passage; EV, empty vector infected; CTR, non-irradiated. (**a**, **c**-**e**), n = 3 independent biological samples, repeated in 2 independent experiments. (**a**, **c**, **d**) Data are mean ±s.d. **P* ≤ 0.05, ***P* ≤ 0.01, unpaired two-sided *t*-tests. Exact *P* values can be found in the accompanying Source Data.

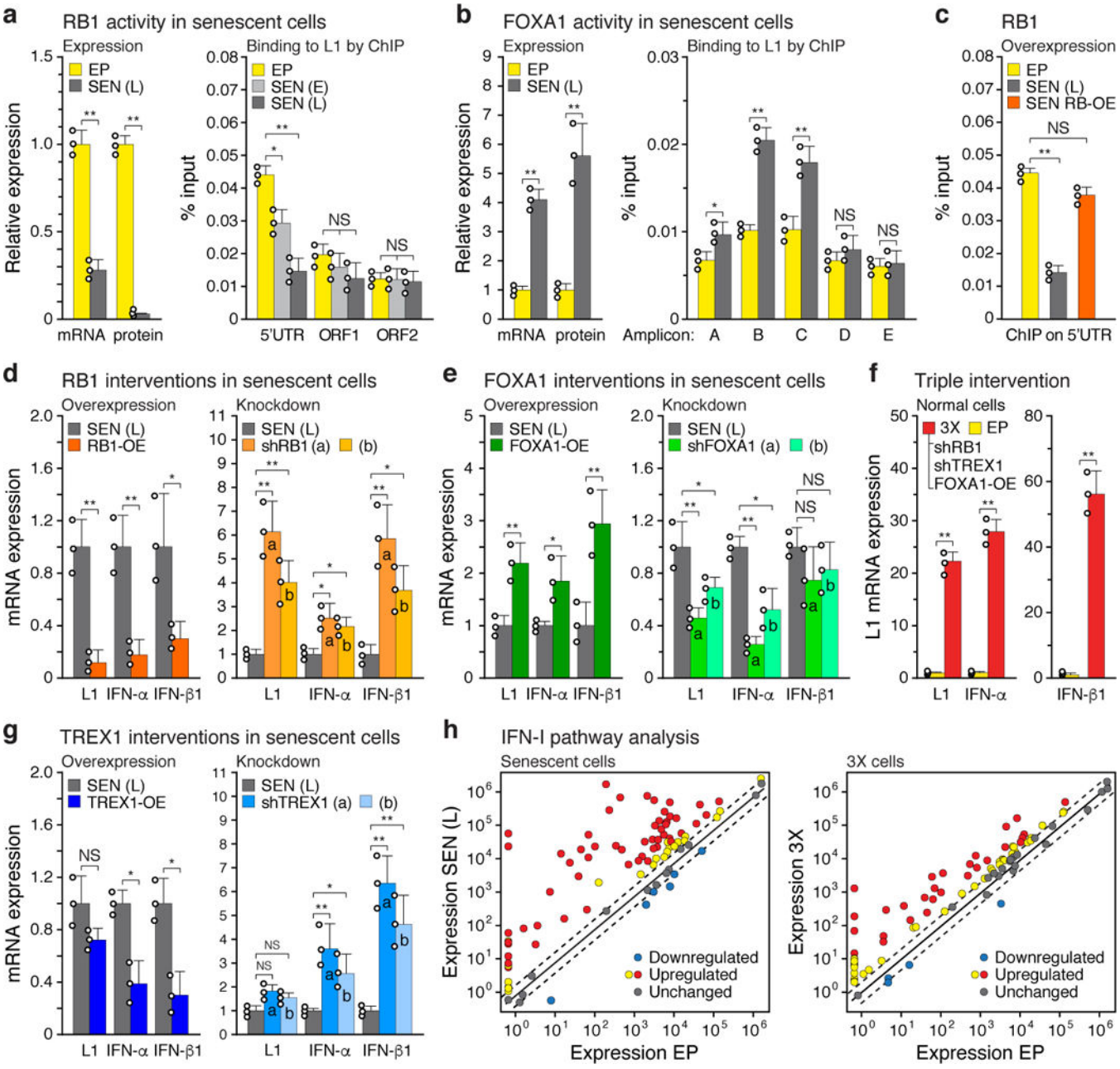


**Figure 2 |. Regulation of L1 activation and IFN-I induction.**

**a,** Expression and ChIP of RB1 and **b,** FOXA1. Expression was measured by RT-qPCR and immunoblotting (left panels). Binding to L1 elements was assessed with ChIP-qPCR (right panels). For primer locations see Fig. 1b. RB1: 5'UTR, ORF1 and ORF2, primers for amplicons A, E and F, respectively. FOXA1: primers for amplicons A-E. qPCR was normalized to input chromatin. SEN (E), early senescence (8 weeks). For gel source data see Supplementary Fig. 1. **c-e,** RB1, FOXA1 or TREX1 were overexpressed (OE) or ablated with shRNAs and the effects on expression of L1, IFN-α and IFN-β1were determined by RT-qPCR of poly(A)-purified RNA. In all cases lentiviral vectors were used to deliver the interventions directly into senescent cells at 12 weeks (point D, Extended Data Fig. 1a), and

cells were harvested for analysis 4 weeks later (point E, 16 weeks). Controls were uninfected senescent cells harvested at the same time (point E, 16 weeks). Two distinct shRNAs (a, b) were used for each gene. Primers for amplicon F were used for L1. **f,** RB1 was overexpressed as above and its binding to the 5'UTR was assessed by ChIP-qPCR (amplicon A). **g,** Activation of L1, IFN-α and IFN-β1 expression after the triple (3X) intervention using shRB1 (a), shTREX1 (a) and FOXA1-OE in early passage cells. Lentiviral infections were performed sequentially with drug selections at each step (shRB1, puromycin –> shTREX1, hygromycin –> FOXA1-OE, blasticidin). **h,** Expression of IFN-I pathway genes was determined with the RT$^2$ Profiler PCR array (Qiagen). Normalized mean expression is shown for all 84 genes in the array. Red symbols: significantly upregulated genes. Dashed lines demarcate the ±2-fold range. (**a**, **b, h**), n = 3 independent biological samples, repeated in 2 independent experiments. (**c**-**g**), n = 3 independent experiments. (**a**-**g**) Data are mean ±s.d. *$P \leq 0.05$, **$P \leq 0.01$, unpaired two-sided *t*-tests. Exact *P* values can be found in the accompanying Source Data.

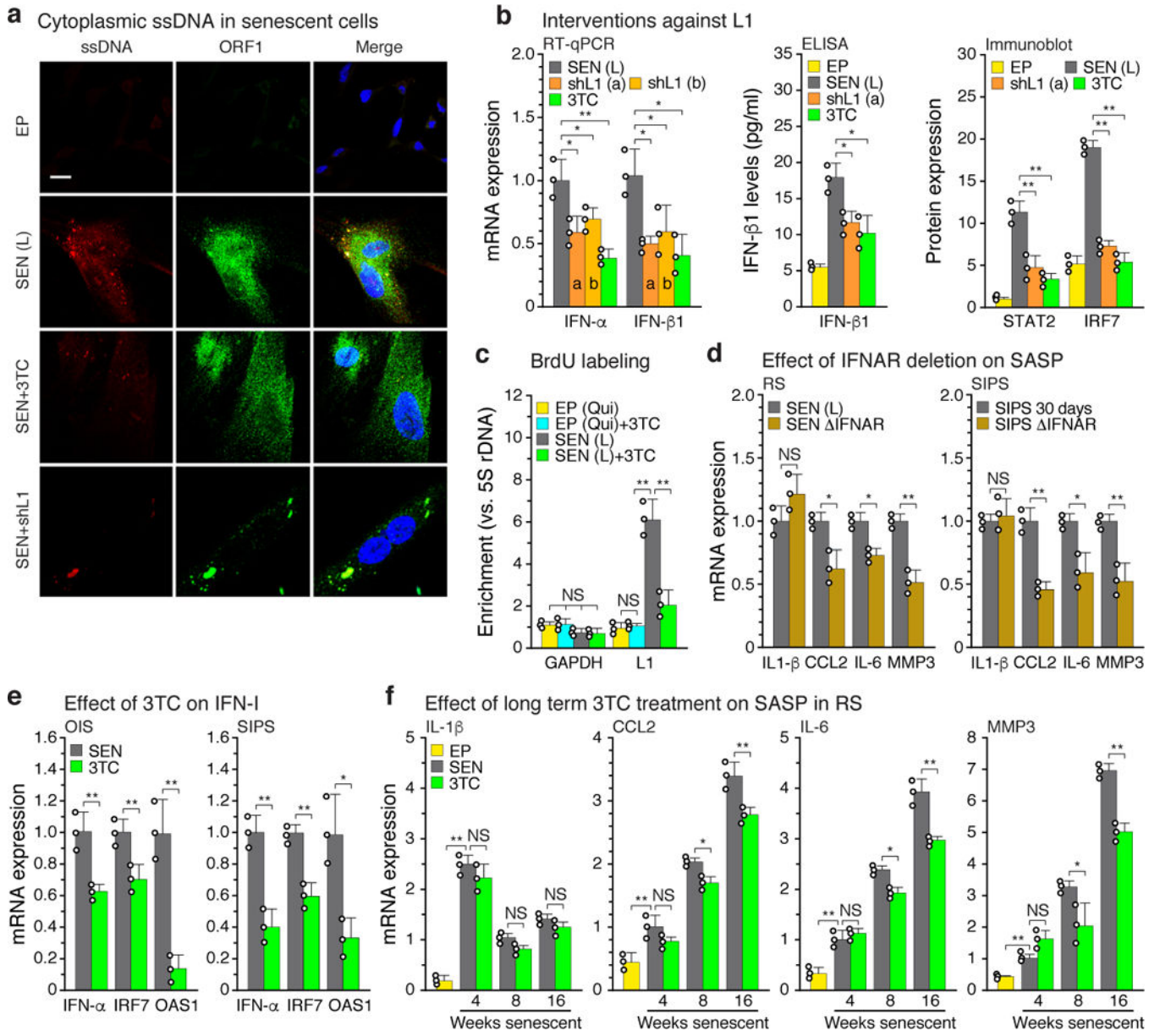


**Figure 3 |. Ablation of L1 relieves IFN-I activation and blunts the SASP response.**

**a,** Cells were examined by immunofluorescence (IF) microscopy using antibodies to single-stranded DNA (ssDNA) or L1 ORF1 protein. Note the bright ssDNA puncta in senescent cells that colocalized with prominent puncta of ORF1. The experiment was independently repeated 3 times with similar results. Scale bar = 10 μm. **b,** Senescent cells were treated with L1 shRNAs (using lentiviral vectors as described in Fig. 2c, e, f) or with 3TC (7.5 μM) between 12 and 16 weeks of senescence. Effects on the IFN-I response were determined by RT-qPCR, ELISA or immunoblotting. For gel source data see Supplementary Fig. 1. **c,** Cells were labeled with BrdU for 2 weeks (with or without 7.5 μM 3TC), labeled DNA was immunoprecipitated, and its L1 sequence content was quantified using a TaqMan multiplex qPCR assay[16] (Fig. 1b, amplicon F). EP (qui), early passage quiescent cells. **d,** Left panel, RS cells: IFNAR1 and IFNAR2 genes were mutagenized using the CRISPR/Cas9 system

delivered with lentivirus vectors directly into senescent cells. As with shRNA interventions, cells were infected at 12 weeks and harvested at 16 weeks of senescence (Fig. 1d-f, Methods). Right panel, SIPS cells: CRISPR/Cas9 intervention was performed in early passage cells and a validated clone was irradiated to induce SIPS. **e,** OIS and SIPS were induced as in Fig. 1d and cells were harvested 20 days (OIS) or 30 days (SIPS) later. 3TC (7.5 μM) was present throughout. IFN-I gene expression (IFN-α, IRF7, OAS1) was measured by RT-qPCR. **f,** Cells were serially passaged into replicative senescence (RS) with 3TC (10 μM) present throughout, and the temporal induction of SASP response genes (IL-1β, CCL2, IL-6, MMP3) was assessed. (**b**-**d**, **f**), n = 3 independent experiments. (**e**) n = 3 independent biological samples, repeated in 2 independent experiments. (**b**-**f**) Data are mean ±s.d. *$P \leq 0.05$, **$P \leq 0.01$. (**b**, **d**-**f**) unpaired two-sided *t*-tests, (**c**) 1-way ANOVA with Tukey's multiple comparisons test. Exact *P* values can be found in the accompanying Source Data.

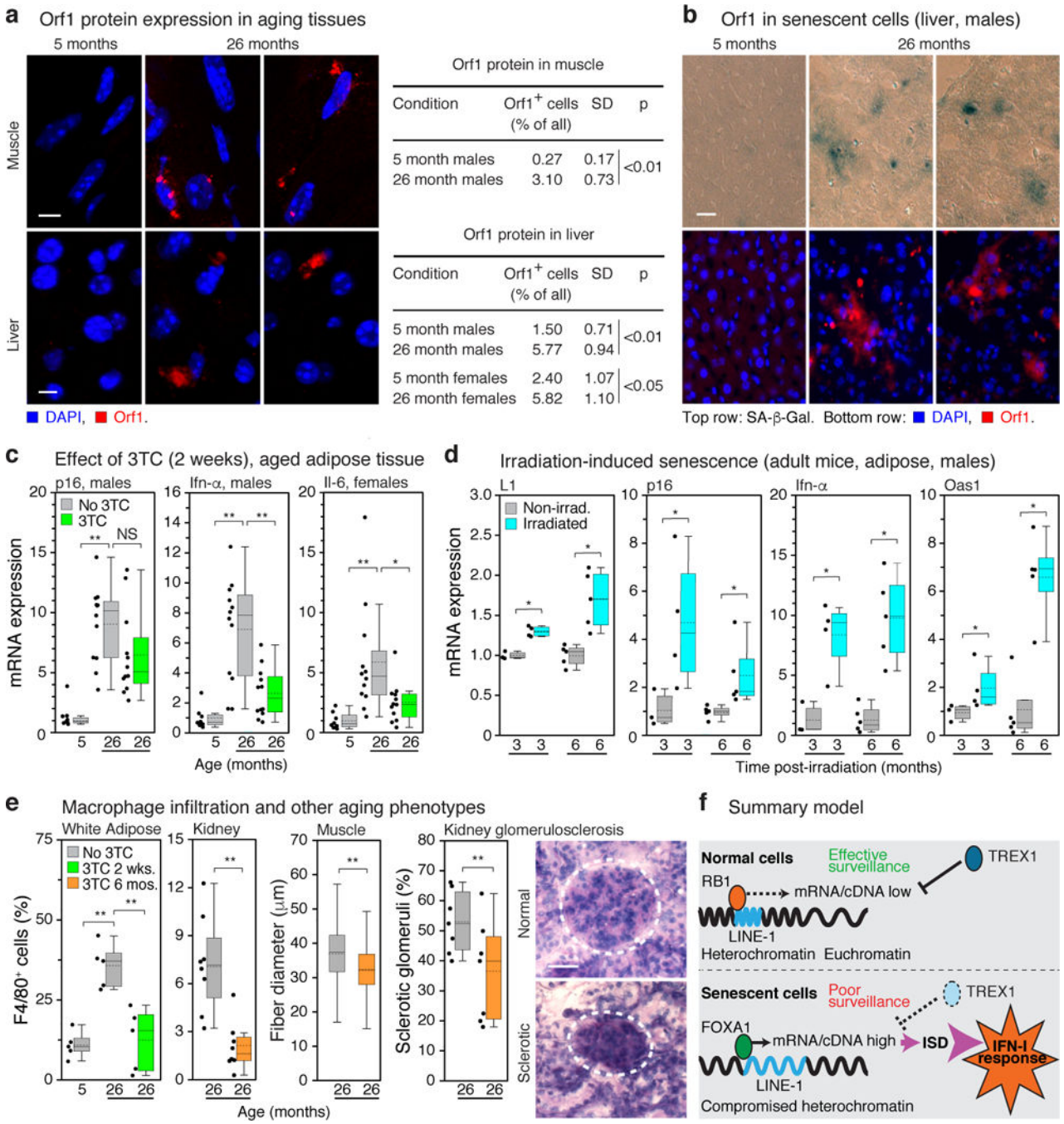


**Figure 4 |. L1s are activated with age in murine tissues and the IFN-I proinflammatory response is relieved by NRTI treatment.**

**a,** Presence of L1 Orf1 protein in tissues was examined by IF microscopy. Quantification of ORF1 expressing cells is shown in the right panel; 3 animals and at least 200 cells per animal were scored for each condition. Scale bar = 4 μm. **b,** Activation of L1 in senescent cells was examined by co-staining for SA-β-Gal activity and Orf1 protein by IF (male liver, 5 and 26 months). Scale bar = 4 μm. The experiment was repeated 3 times independently with similar results. **c,** Mice were administered 3TC (2 mg/ml) in drinking water at the

indicated ages for two weeks and sacrificed after treatment. Expression of p16, an IFN-I response gene (Ifn-α), and a marker of a proinflammatory state (Il-6) were assessed by RT-qPCR. See Extended Data Fig. 9 for additional tissues and genes. The box plots show the range of the data (whiskers), 25th and 75 percentiles (box), means (dashed line), and medians (solid line). Each point represents one animal. 5 months, n = 8; 26 months, n = 12; 29 months, n = 6. **d,** Six month old mice were non-lethally irradiated and expression of L1, p16 and representative IFN-I response genes (Ifn-α, Oas1) were assessed by RT-qPCR at the indicated times post-irradiation. Graphical presentation is as in (c); non-irradiated, n = 3 animals at 3 months, n = 5 animals at 6 months; irradiated, n = 4 animals at 3 months, n = 5 animals at 6 months. **e,** Macrophage infiltration into white adipose tissue and kidney was scored as F4/80 positive cells (% of total nuclei). n = 5 animals group (adipose); n = 8 (kidney). Skeletal muscle fiber diameter was measured (Methods) and plotted as an aggregate box plot. n = 5 animals per group, 500 fibers total. Glomerulosclerosis was scored in periodic acid-Shiff (PAS)-stained sections (Methods) as the sum of all glomeruli with a score of 3 or 4 divided by the total. n = 7 animals per group, 40 glomeruli per animal. Graphical presentation is as in (c). 3TC treatment was 2 weeks for white adipose and 6 months (20–26 months) for other tissues. Dashed circle demarcates a single glomerulus. Scale bar = 50 μm. **g,** Breakdown of L1 surveillance mechanisms leads to chronic activation of the IFN-I response. ISD: interferon-stimulatory DNA pathway. (**a**, **d, e**) unpaired two-sided *t*-tests. (**c**, **e** white adipose) 1-way ANOVA with Tukey's multiple comparisons test. Exact *P* values can be found in the accompanying Source Data.